YIELDS OF FISSION-RECOIL BROMINE BY DELAYED-NEUTRON STUDIES

YIELDS OF FISSION-RECOIL BROMINE BY DELAYED-NEUTRON STUDIES

by

MARVIN DAVID SILBERT, B.Sc.

A Thesis

Submitted to the Faculty of Graduate Studies

in Partial Fulfilment of the Requirements

for the degree

Doctor of Philosophy

McMaster University

May 1965

DOCTOR OF PHILOSOPHY (1965) McMASTER UNIVERSITY
(Chemistry)

TITLE: Yields of Fission-Recoil Bromine by Delayed-Neutron Studies

AUTHOR: Marvin David Silbert, B.Sc. (McMaster University)

SUPERVISOR: Dr. R.H. Tomlinson

NUMBER OF PAGES: x, 112

SCOPE AND CONTENTS: Fission-product bromine was isolated from a uranium target by the hot-atom reaction of the fission recoils with methane to form organic bromides. The organically-bound bromine was shown to be formed preferentially by primary (independently-formed) bromine with little contribution from secondary bromine.

The delayed-neutron activity of the short-lived bromine isotopes was analyzed to obtain the relative yields of delayed-neutrons from Br^{87}, Br^{88} and Br^{89} produced as primary fission products. The relative delayed-neutron yields are summarized below.

	Br^{87}	Br^{88}	Br^{89}
U^{233}	0.55 ± 0.2	1.0 ± 0.1	0.6 ± 0.1
U^{235}	0.32 ± 0.3	1.0 ± 0.1	1.2 ± 0.1

The primary yields of the three isotopes in fission were estimated on the basis of their delayed-neutron yields.

ACKNOWLEDGEMENTS

I would like to express my appreciation to all those who made this research possible:

To my research director, Dr. R. H. Tomlinson, for giving me complete freedom to pursue this project on my own. I would like to thank him for his advice and encouragement throughout the course of this work.

To the reactor supervisory staff: Dr. W. H. Fleming, J. B. McDougall and P. Ernst and to the reactor operating staff: W. Griffith, S. Hallewell, G. Hanas , R. Jarrett, K. Marshall, D. Maystruk, T. Noakes and J. Walling for their cooperation, assistance and advice.

To Dr. A. K. Das Gupta of the Department of National Health and Welfare, Ottawa, and Dr. D. W. Ockenden of the U.K.A.E.A. Windscale for their work in the design and construction of the reactor beam port. A special thanks to Dr. Ockenden for his design of the mechanical shutter.

To T. Bryden and the staff of the research shop for their valuable help in the construction of the irradiation facility.

To N. P. Archer who taught me the intricacies of computing. I would like to thank him for the advice that was always available.

To the Health Physics staff, D. Whiteford and A.J.J. Roncari, with whom I shared a laboratory throughout the course of this work, for their help and advice.

To Dr. J. Fiedler for helpful discussions and for making available to me his Z_p values.

To the staff of the 7040 computer for running my programs and for their help when the programs would not run.

To Mrs. H. Kennelly for a wonderful job in typing this thesis. Without her help this thesis could not have made the deadline.

To my family for encouragement throughout this work.

To the National Research Council who supported this work and to McMaster University and the Province of Ontario for scholarships which supported me.

And finally, my thanks to J. Pleva, M. Azeem, The Crystallography Group, J. Kitching, F. Hainsworth, D. Slavinskas, J.Crabb, F. Kastner, and the many other people who have helped me throughout my stay at McMaster.

TABLE OF CONTENTS

LIST OF TABLES

LIST OF FIGURES

CHAPTER I

INTRODUCTION

(i) Historical Introduction

Within a month after the discovery of fission by Hahn and Strassman (1) in 1939, Fermi (See Szilard and Zinn (2)) suggested that some of the fission fragments having undergone one or more beta decays could emit delayed neutrons. The theory of fission postulated by Bohr and Wheeler (3) and by Frankel (4) supported Fermi's prediction by showing that sufficient energy could be available following beta decay to exceed the binding energy of the most loosely bound neutron and hence, permit neutron emission.

The first experimental evidence for delayed-neutron emission was given by Roberts et al (5). They observed a neutron activity decaying with a half-life of 12.5 ± 3 seconds. The high yield of this "delayed" neutron activity confirmed that the activity was due to delayed-neutron emission rather than photo-neutron emission.

Many subsequent studies have been made of the delayed-neutrons in fission, measuring their half-lives, abundances, and energies; a number of these have been summarized by Keepin (6,7,8) and Hyde (9). The most extensive studies of the abundances and half-lives were those of Keepin (10) and Hughes (11). Keepin et al (10) measured the delayed-neutron yields from a number of fissioning nuclides and by means of a least-squares computer technique separated the delayed-neutron yields into six half-live groups; their yield data from thermal-neutron fission of U^{233} and U^{235} are shown in Table I. Table II shows the mean energies of the delayed-

TABLE I

Thermal-fission delayed-neutron data of Keepin, Wimett and Zeigler (10)

Group Index i	Half-life, T_i (sec.)	Relative abundance, a_i/a	Absolute group yield (%)
	U^{235} (99.9% 235; n/F = 0.0158 ± 0.0005)		
1	55.72 ± 1.28	0.033 ± 0.003	0.052 ± 0.005
2	22.72 ± 0.71	0.219 ± 0.009	0.346 ± 0.018
3	6.22 ± 0.23	0.196 ± 0.022	0.310 ± 0.036
4	2.30 ± 0.009	0.395 ± 0.011	0.624 ± 0.026
5	0.610 ± 0.083	0.115 ± 0.009	0.182 ± 0.015
6	0.230 ± 0.025	0.042 ± 0.008	0.066 ± 0.008
	U^{233} (100% 233; n/F = 0.0066 ± 0.0003)		
1	55.0 ± 0.54	0.086 ± 0.003	0.057 ± 0.003
2	20.57 ± 0.38	0.299 ± 0.004	0.197 ± 0.009
3	5.00 ± 0.21	0.252 ± 0.040	0.166 ± 0.027
4	2.13 ± 0.020	0.278 ± 0.020	0.184 ± 0.016
5	0.615 ± 0.242	0.051 ± 0.024	0.034 ± 0.016
6	0.277 ± 0.047	0.034 ± 0.014	0.022 ± 0.009

TABLE II

Mean energies of the delayed-neutron groups for U^{235}

Group index	$T_{1/2}$(sec)	Hughes (11) Argonne (kev)	Burgy (12) Oak Ridge (kev)	Batchelor (15) Harwell (kev)
1	54	250 ± 60	300 ± 60	250 ± 20
2	22	560 ± 60	670 ± 60	460 ± 10
3	5.9	430 ± 60	650 ± 100	405 ± 20
4	2.2	620 ± 60	910 ± 90	450 ± 20
5	0.46	420 ± 60	---	---
6	0.13	---	---	---

neutron groups; these have been measured by cloud chamber (5,12,13) and "age" measurement (11,14) techniques and calculated from the energy spectra measured by Batchelor and Hyder (15) using a He^3 proportional counter (16).

The first chemical separation of the short-lived fission-product halogens was performed by Hahn and Strassman (17). They observed a bromine activity and an iodine activity of half-lives 50 ± 9 seconds and 30 ± 6 seconds respectively. Later works (18,19) assigned masses 87 and 137 respectively to these activities. Snell et al (20) identified these two isotopes as the precursors of the 55 second and 22 second delayed-neutron activities.

The most extensive chemical study of the delayed-neutron precursors has been performed by Perlow and Stehney (22). Using very fast wet-chemical and counting techniques, they showed that with the exception of the 55 second period, each half-life group contained at least one bromine and one iodine isotope. Table III gives the bromine and iodine isotopes shown by Perlow and Stehney to contribute to the various half-life groups. The relative yields of these isotopes are given in Table IV.

(ii) Aim of this Work

The previous workers have chemically identified the main fission-product delayed-neutron precursors and have measured their half-lives and abundances in various fissioning systems. The abundances which have been measured consist of two parts; a primary fraction from precursors which are primary fission products, and a secondary fraction from precursors formed by beta decay.

TABLE III

Halogen Delayed-Neutron Activities
(Data of Perlow and Stehney (22))

Delayed-Neutron Period	Identified Delayed-Neutron Precursor	Half-Life
55 seconds	Br^{87}	54.5 seconds
22	Br^{88}	16.3
	I^{137}	24.4
6	Br^{89}	4.4
	I^{138}	6.3
2	Br^{90}	1.6
	I^{139}	2.0

TABLE IV

Relative Yields of Halogen Delayed-Neutron Activities from U^{235}
(Data of Perlow and Stehney (22))

Element	Isotope	Relative Yield*
Bromine	87	0.37
	88	1.0
	89	1.9
	90	1.5
Iodine	137	1.0
	138	0.47
	139	0.38

* Bromine yields normalized to Br^{88}; Iodine yields normalized to I^{137}

It was the purpose of this work to measure the abundances of the primary fraction alone using as an isolation technique the hot-atom reaction of fission-recoil bromine with methane. Measurements were made of the abundances of delayed neutrons from Br^{87}, Br^{88} and Br^{89} produced as primary fission products in the thermal-neutron fission of U^{233} and U^{235}. The measured abundances were corrected for neutron-emission efficiencies in order to obtain the relative primary yields of the three bromine isotopes; these yields are compared with various theoretically predicted yields.

CHAPTER II

THEORETICAL

(i) Delayed-Neutron Emission

As a result of beta decay, some nuclei are left with an excitation energy exceeding the binding energy of the most loosely bound neutron. The excitation energy can be lost by emission of this neutron to yield the isotope one mass unit lighter.

The neutron emission is a fast process, but can occur only as rapidly as the neutron-emitting states are populated. The beta decay governs the rate at which these states are populated and, hence, the rate at which neutron emission occurs. The neutron emission will, thus, appear to be a "delayed" process with a decay rate the same as that of its beta-decaying precursor.

The term "delayed-neutron emission" is given to this phenomena. A "delayed-neutron precursor" is the nucleus which undergoes beta decay to the excited levels of the "delayed-neutron emitter" which emits "delayed neutrons".

The delayed-neutron emission process is shown schematically in Fig. 1. The delayed-neutron precursor Z^A, undergoes beta decay populating various levels in the delayed-neutron emitter, $(Z + 1)^A$. Those levels above the neutron binding energy B_n can de-excite themselves either by delayed-neutron emission to the ground state(or excited states) of $(Z + 1)^{A-1}$ or by gamma emission to the ground state of $(Z + 1)^A$. It is the former process with which this work is involved.

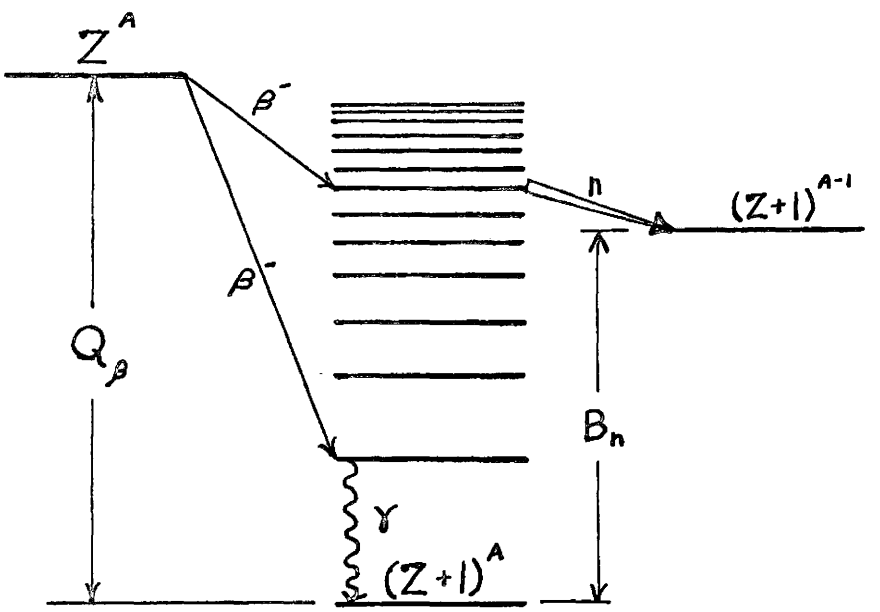

DELAYED – NEUTRON EMISSION

(SCHEMATIC REPRESENTATION)

Fig. 1

The levels below B_n will depopulate themselves by gamma emission to the ground state of $(Z + 1)^A$. No delayed-neutron emission can occur from these levels since insufficient energy is available.

Delayed-neutron emission would be expected to occur in nuclides which have low neutron binding energies. The neutron binding energy just above closed neutron shells is lower than in other regions; most of the known delayed-neutron emission occurs in this region as shown in Table V. One exception is $Li^9(23)$, whose daughter nucleus has a weakly bound neutron added to a very stable even-even configuration (two alpha particles).

The diagram shown in Fig. 1 represents the Bohr-Wheeler (3) desciption of delayed-neutron emission. The probability that a beta decay will lead to neutron emission can be evaluated from beta decay theory.

From the Fermi theory of beta decay, it can be shown that the probability density that a nucleus will undergo a beta transition to an energy level E, is given by equation (1)

$$\omega(E) = C|M|^2 \; f \; (Z + 1, Q_\beta - E) \; \rho(E) \; dE \quad . \quad (1)$$

C is constant.

M is a matrix element of the beta transition. In the absence of appropriate wave functions for the initial and final states, M can only be estimated. In the region of excitation where delayed-neutron emission occurs, the density of levels is very high. If the assumption is made that M has no large systematic variation with energy, $|M|^2$ can be replaced by its average(constant) value. $|M|^2$ is, on the average, two orders of magnitude lower for forbidden transitions than for allowed transitions; it can be assumed that allowed transitions predominate.

TABLE V

Occurrence of Delayed-Neutron Emitters

Delayed-Neutron Emitter	Precursor	Mass	Closed Neutron Shell	Excess Neutrons above closed shell
O	N*	17	8	1
Kr	Br	87	50	1
		88		2
		89		3
		90		4
Xe	I	137	82	1
		138		2
		139		3
Pb	Tl**	210	126	2

* (24, 25, 26)

** (27)

$f(Z + 1, Q_\beta - E)$ is a "Fermi-Function". It is a non-analytical integral related to the total energy $(Q_\beta - E)$ integrated over the whole beta spectrum. It has been evaluated by Feenberg (28) and Moszkowski (29).

Q_β is the total energy available for beta decay. It is the difference in energy between the ground states of the parent and daughter nuclei. In the case of the fission-product delayed-neutron precursors Q_β has been determined only for Br^{87*} (15, 30, 31). Q_β and B_n can be estimated for the other nuclides from beta-decay systematics (32, 33) or neutron binding-energy systematics (34, 35, 36).

$\rho(E)$ is the density of levels in the daughter nucleus. The level density has been formulated by Blatt and Weisskopf (37) and is of the form shown in equation (2).

$$\rho(E) = C \exp\left[2(aE)^{1/2}\right] \qquad (2)$$

C and a are constants.

For Br^{87} in the region above the neutron binding energy, the level density is very high and evaluation of equation (2) yields densities in the order of 10^3 to 10^4 levels per MeV. It is unlikely, however, that all of these levels will be populated.

The probability that a neutron will be emitted from a given excited state of the delayed-neutron emitter is given by equation (3).

$$p_n = \Gamma_n / (\Gamma_n + \Gamma_\gamma). \qquad (3)$$

The Γ's refer to the level widths or probabilities for neutron and gamma emission; they have been evaluated by Feshbach (38).

---

* Stehney's (30) value will be in error as it contained Br^{86} which was unknown at that time. (Discovery of Br^{86}, A. F. Stehney and E. P. Steinberg, Phys. Rev. 127, 563 (1962))

For the bromine isotopes and neutrons of angular momentum $\ell = o$ or 1, p_n is zero below the neutron binding energy. It rises to unity in the first 50 keV. Above this energy p_n remains at unity, making neutron emission the only mode of decay. Neutron emission and gamma emission are competitive processes between B_n and $B_n + 50$ keV. Below B_n gamma decay is the only mode of decay.

Multiplication of the beta transition probability, equation (1), by the neutron emission probability, equation (3), and integration between the limits B_n and Q_β gives N_n, the number of neutron-emitting states.

$$N_n = C \int_{B_n}^{Q_\beta} f(Z + 1, Q_\beta - E) \rho(E) \frac{\Gamma_n}{\Gamma_n + \Gamma_\gamma} dE \qquad (4)$$

The total number of beta decays is obtained by integration of equation (1) between the limits zero and Q_β.

$$N_\beta = C \int_{0}^{Q_\beta} f(Z + 1, Q_\beta - E) \rho(E) dE . \qquad (5)$$

Division of N_n by N_β yields the fraction of beta decays which lead to neutron emission.

$$P_n = \frac{\int_{B_n}^{Q_\beta} f(Z + 1, Q_\beta - E) \rho(E) \frac{\Gamma_n}{\Gamma_n + \Gamma_\gamma} dE}{\int_{0}^{Q_\beta} f(Z + 1, Q_\beta - E) \rho(E) dE} \qquad (6)$$

P_n is the neutron-emission probability of the delayed-neutron precursor. Table VI shows the neutron-emission probabilities of the fission product halogens. These have been measured by Aron et al (39).

TABLE VI

Neutron-Emission Probabilities*

Precursor	Half Life (sec)	Neutron-Emission Probability U-238	Th-232
Br^{87}	56	0.031 ± 0.006	0.031 ± 0.006
Br^{88}	16	0.06 ± 0.016	0.06 ± 0.016
Br^{89}	4.3	0.07 ± 0.02	0.07 ± 0.02
I^{137}	24	0.030 ± 0.005	0.030 ± 0.005
I^{138}	6.3	0.019 ± 0.005	0.021 ± 0.005

*Aron (39)

The mathematical model presented here is very much simplified. All energies have been measured from the ground state and are thus subject to even-odd and shell effects. Calculations should be made from a "characteristic level", an artificial level which is sufficiently high to avoid even-odd and shell effects. An extended treatment of delayed-neutron theory using the characteristic-level treatment has been presented by Keepin (40).

(ii) Delayed Neutrons and Fission

a. The Fission Process

Nuclear fission is a process whereby a heavy nucleus splits into two or more medium-mass fragments (fission products) accompanied by the release of a large quantity of energy mainly as recoil energy given to the fission fragments. The events in the fission process may be tabulated as follows:

0. Excitation of the nucleus.
1. Fission; the fragments begin to separate.
2. Fission fragments acquire most of their kinetic energy. (Kinetic energy comes from coulombic repulsion between the fragments).
3. Fragments lose excitation energy by emission of "prompt" neutrons.
4. Fragments lose energy by emission of "prompt" gamma rays.
5. Fragments come to rest having been slowed down by the stopping material.

With the heaviest elements, fission takes place spontaneously; it can be their principal mode of decay. This is the case with nuclides such

as Cf^{252} and Fm^{256}. With elements of lower mass, the spontaneous fission process is much less favoured; the principal mode of decay is by alpha or beta emission. The fission process can be enhanced in these nuclides by addition of excitation energy by bombardment with neutrons, protons, etc. of low or moderate energy. U^{235}, U^{238}, Th^{232}, Pu^{239} and many others can be induced to undergo fission in this manner. Very high excitation (above 50 MeV and up into the GeV region) can induce fission in much lighter elements such as lead, gold and some of the rare earths.

The mass distribution of the fission fragments varies both with the fissioning nuclide and with the excitation energy. Low excitation energies give the familiar double-humped mass-yield curve representing asymmetric fission. As the excitation energy increases, symmetric fission begins to appear, and becomes the predominant mode at very high excitations.

The fission products lie over a broad range of masses. Thermal-neutron fission of U^{235} produces a distribution of products ranging in mass from 70 to 160 with low mass and high mass maxima* at 95 and 139 respectively. Changing the mass of the fissioning nuclide causes a large shift in the distribution of the low mass group and a much smaller shift in the high mass group. Fast fission of Th^{232} and spontaneous fission of Cf^{252} have low mass maxima at 92 and 108 respectively; the high mass maxima are at 139 and 142 respectively.

The fissioning nucleus has a high ratio of neutrons to protons; the fission fragments also have this high ratio of neutrons to protons. This excess of neutrons makes the fission products unstable and leads to furth-

---

*Maxima estimated neglecting fine structure in mass-yield curve. Yield data for Th^{232}, U^{235} by Katkoff (41) and Cf^{252} by Nervik (42).

er decay by beta emission.

The fission products can be divided into two classes depending upon the mode of formation.

Primary Fission Products: These are the nuclei produced directly by the fission act itself. They are fission fragments which have undergone prompt-neutron and prompt-gamma emission, but have not undergone beta decay. They are often referred to as "independent" fission products.

Secondary Fission Products: These nuclei are not produced directly by the fission act; they are produced by beta decay of other fission products. Their precursors may be either primary or secondary fission products.

It should be pointed out that a given nucleus can be produced by both methods; it can be both a primary fission product and a secondary fission product. As an example, Br^{87} is produced by both methods.

$$U^{235} \quad (n,F) \quad Br^{87}$$

$$U^{235} \quad (n,F) \quad Se^{87} \xrightarrow{\beta} Br^{87}$$

$$U^{235} \quad (n,F) \quad As^{87} \xrightarrow{\beta} Se^{87} \xrightarrow{\beta} Br^{87}$$

In the first case, Br^{87} is a primary fission product; in the second and third cases, it is a secondary fission product. The yield consists of two parts: the primary (or independent) yield and the secondary yield; the total yield is the sum of both.

A complete theory of the fission process has not yet been reported. Several attempts have been made to produce a "working" theory using mathematical models. The most notable theories have been: The liquid-drop model of Bohr and Wheeler (3) and Frankel (4), the statistical model of

Fong (43) and the unified model of Bohr (44). Hyde (9) has published a review of fission giving the present (1962) state of theoretical calculations and experimental measurements. With the complexity of the fission process, it is unlikely that a complete theory will be available in the near future.

b. Delayed-Neutrons from Fission

Fission produces a number of nuclides which lie in the region just above the N=50 and N=82 closed shells and are delayed-neutron precursors. One to two percent of all fissions lead to delayed-neutron emission. Short-lived halogens have been identified as the major* contributors to delayed-neutron emission in fission; other nuclei have been predicted, but not yet studied. Table VII shows the predicted and presently known delayed-neutron precursors.

Cumulative fission-yields are affected by delayed-neutron emission. The mass chain of the delayed-neutron precursor will have a lowered yield because of its loss to the next lighter chain. The latter chain will have an increased yield because of its gain from its precursor. Corrections for delayed-neutron emission must be considered when evaluating cumulative fission yields.

c. Role of Delayed Neutrons in Reactor Control

Delayed neutrons, although of very small yield from fission, are of great importance; they make possible the control of a nuclear chain reaction. Without delayed neutrons, it would be impossible to safely

---

* Kristyuk (45) has calculated the total yields of the bromine and iodine delayed-neutron precursors in U^{238}. He has assessed their contribution to the total delayed-neutron emission to be no more than 20%.

TABLE VII

Delayed-Neutron Precursors in U^{235} Fission+

Group Number (6 groups)		Precursor * Assignment
1	54.5 sec.	Br^{87}
2	24.4	I^{137}
	16.3	Br^{88}
3	6.3	I^{138}
	4.4	$Br^{(89)}$
	~6	$Rb^{(93,94)}$
4	2.0	I^{139}
	(1.6 - 2.4)	(Cs, Sb, or Te)
	1.6	$Br^{(90-92)}$
	~1.5	$Kr^{(93)}$
5	~0.5	(I^{140} + Kr?)
6	~0.2	(Br, Rb, As, ?)

+ Table taken from Keepin (8)

* Tentative assignments in parentheses (cf Keepin (40))

harness the energy produced from nuclear fission.

In order to operate a nuclear reactor at a constant power level, the number of neutrons produced in one generation must equal the number produced in the preceding generation. The multiplication factor, k, is defined as the ratio of the former to the latter. Any excess of k over unity will cause a rise in power; the excess, k-1, is known as the excess reactivity, δk.

If δk is greater than zero, the reactor will rise in power; the rate of rise in power (or number of neutrons) is given* by equation (7):

$$\frac{dN}{dt} = \frac{N}{T} \qquad (7)$$

N is the number of neutrons present and T is the reactor period defined in terms of the excess reactivity and the neutron lifetime in the reactor, ℓ.

$$T = \ell/\delta k \qquad (8)$$

Integration of (7) yields:

$$N = N_o e^{t/T} \qquad (9)$$

t is time and N_o is the initial power or number of neutrons initially present.

The reactor period, equation (8) is based solely upon prompt neutrons; no contribution for delayed neutrons is included. A reactor period, including a delayed-neutron term, has been defined:

$$T_{delayed} = \frac{\ell + (\bar{\beta} - \delta k)\bar{\tau}}{\delta k} \qquad (10)$$

$\bar{\tau}$ is the mean lifetime of the delayed neutrons and $\bar{\beta}$ is the delayed-

*Derivations from Murray (46)

neutron fraction; their contribution to the total number of neutrons.

Evaluation of the reactor period and power increase for a typical* reactor shows the importance of delayed neutrons. The values are shown below for a small excess reactivity of one quarter of one percent.

	Reactor Period	Relative Power Increase (per second)
Prompt neutrons alone	0.08 seconds	3×10^5
Prompt plus delayed neutrons	25 seconds	1.04

Operation, based solely upon prompt neutrons, yields a very short period. Control mechanisms must be very rapid in order to control the rate of fission. If the operation is also based upon a delayed-neutron component, the control need not be as fast due to the lengthened period.

(iii) Hot-Atom Chemistry

a. Introduction

Hot-atom chemistry is the chemistry of atoms which are not in thermal equilibrium with their environment, but have a very high "local" temperature. They can be produced by irradiation with ultra violet or ionizing radiation or by nuclear processes.

Hot-atom reactions may be distinguished from thermal chemical reactions by the following criteria:

(a) They are temperature independent. The nature of a hot-atom reaction is dependent upon its local temperature. This temperature is usually much higher than that of the thermal environment; thus,

---

* Example given by Murray (46) has neutron lifetime of 2×10^4 seconds; values of $\bar{T}$ and $\bar{\beta}$ are 12.2 seconds and 0.00755 respectively from thermal fission of U^{235} (14).

the hot-atom reaction will be independent of the temperature of its surroundings. The high "local" temperature allows reactions to proceed which could not normally occur if the reacting species were in thermal equilibrium with their environment as reactions need not follow the route requiring the lowest energy of activation .

(b) Hot-Atom reactions are unaffected by the addition of reactive thermal-radical scavengers. Hot-atom reactions do not occur by recombination of thermalized radicals; they are unique hot-displacement processes. Addition of reactive thermal-radical scavengers will have no effect upon the hot-atom reactions.

(c) The yields of hot-atom reactions are reduced by the addition of inert moderators. Hot-atom reactions occur at high "local temperatures; addition of inert moderators will reduce this high "local" temperature by removing excess kinetic, vibrational and electronic excitations. Reactions can occur only over a short range of energy*. With the addition of moderator, the number of species in the correct energy range is reduced and hence the number of atoms undergoing hot-atom reaction is also reduced.

---

* It is unlikely that fragments can form stable compounds if their kinetic energy greatly exceeds bonding energies. For hot-atom reaction to occur, this energy must, however, exceed the energy of the bonds being broken. Hot-atom reactions are expected to occur in the region between 2 and 5 eV.

Hot-Atoms can be produced by activation with ultra violet and ionizing radiation or by nuclear transformations. The latter method includes both nuclear reactions and nuclear decay.

Ultra violet activation produces the most controlled source of hot atoms; they are well defined in energy. The ranges of energies are, however, very small since they are limited by the absorption of the system and by conservation of momentum during bond rupture. Ionizing radiation is much less selective than ultra violet; it can activate any compound and can produce a variety of excited states.

Nuclear transformations have been the most widely studied hot-atom systems. The hot-atom, produced by a nuclear process, may carry a "label" making it easy to find. Very high kinetic energies and charges are produced by nuclear processes. Table VIII shows the recoil energies available for some representative nuclear processes. The recoil energies available from radioactive decay are shown in Appendix I.

Several reviews have been published describing theories and nature of hot-atom reaction; among these are Willard (47,48,49), Harbottle and Sutin (50) and Wolf (51).

b. Gas-Phase Reactions of Hot Halogens

Extensive studies of gas-phase reactions of hot halogens have been carried out by Willard and others. Willard has published a number of reviews of this work (47, 48, 49). A mathematical model has been presented by Estrup and Wolfgang (52) which can be applied to hot-halogen systems.

Horning (53) reported that iodine atoms activated by the I^{127} (n,γ) I^{128} process reacted with methane to form CH_3I^{128}. One half of the yield

TABLE VIII

Recoil Energies Available from Nuclear Transformations

Initial Nucleus	Nuclear Process	Final Nucleus	Recoil Energy*
Cl^{37}	n,γ	Cl^{38}	510 eV
Br^{81}	n,γ	Br^{82}	230 eV
I^{127}	n,γ	I^{128}	150 eV
Br^{80m}	I.T.	Br^{80}	High Charge**
N^{14}	n,p	C^{14}	40 keV
Li^{6}	n,α	H^{3}	2.7 MeV
U^{235}	n,F	Light Fragment	100 MeV***
U^{235}	n,F	Heavy Fragment	68 MeV***

* n,γ process assumes emission of one gamma ray of energy 6 MeV

** Wexler (54) found very highly charged species. Charges varied from Br^{+} to Br^{13+} with a maximum at Br^{7+}.

*** Measurements by Milton and Fraser (55)

could be attributed to a unique hot-displacement process.

$$I^{*} + CH_4 \longrightarrow CH_3I + H$$

Schroth (55) found similar results using iodine activated by the Xe^{125} (E.C.) I^{125} process. Chien (57) and Gordus (58) found that similar reactions occurred with isotopes of chlorine and of bromine; the efficiency was dependent upon the particular halogen and target compound.

The variation in yield with addition of inert moderators has been studied both for reactions of hot halogens with organic media (Rack (59)) and for reactions of hot tritium with organic media (Estrup (51)). The experiments show that the yield of the reaction diminishes with increasing concentration.

The application of fractional distillation (60,61) and later gas-chromotographic (62,63,64) techniques revealed a large number of products. This large multiplicity of products shows that the hot atoms displace not only the hydrogen, but also radicals and other halogens. Fig. 2 shows a gas chromatogram of the radioactive products of the hot-atom reaction of bromine, activated by the Br^{81} (n,γ) Br^{82} process, in liquid n-propylbromide. The chromatogram taken in this laboratory with the apparatus described by Silbert (64) shows the large multiplicity of products.

Wolfgang and Rowland (65) suggested the application of hot-atom techniques to fission-product halogens as a means of isolating the fission-recoil fragments from the fissioning target. Denschlag et al (66,69) studied the reaction of fission-recoil iodine with methane. Analysis of

---

*The Asterisk, used in chemical reactions, will denote the hot or activated species.

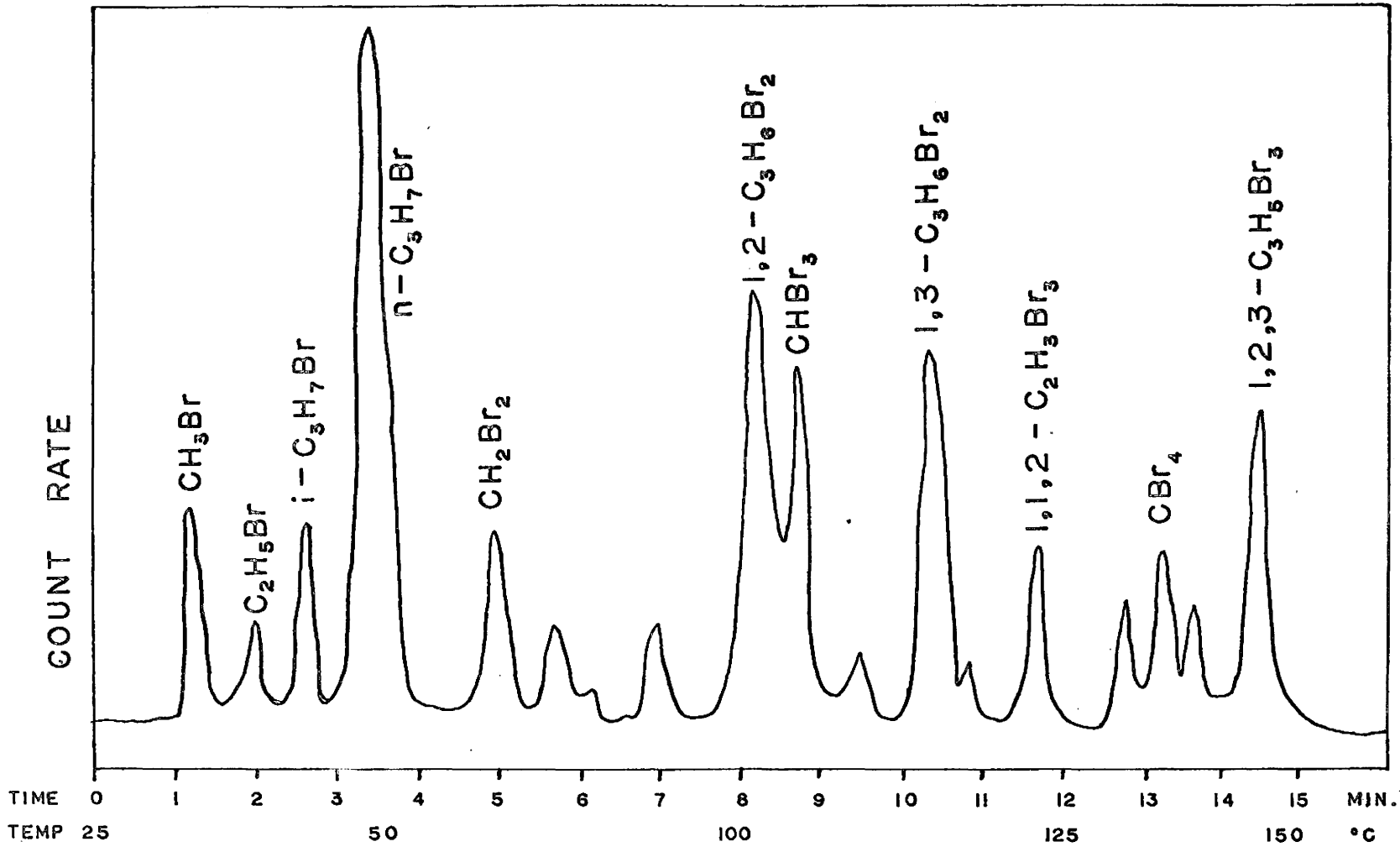

Fig. 2 GAS CHROMATOGRAM OF THE PRODUCTS OF THE $Br^{81}(n,\gamma)Br^{82}$ REACTION IN $n-C_3H_7Br$ PLUS 5 MOLE % Br_2

the organically-bound iodine showed that it consisted mainly of primary fission-product iodine with little interference from secondary iodine.

This work is an extension of that of Denschlag et al (66,69) isolating primary bromine by hot-atom reaction with methane.

CHAPTER III

EXPERIMENTAL APPARATUS

(i) Irradiation Cell

a. Basis of Operation

The operation of the irradiation cell was based upon the hot-atom reaction of the recoiling fission fragments with methane. The recoiling halogen fission fragments were expected to form methyl halides by hot-displacement reactions in the same manner as the neutron-activated species:

$$Br^{*} + CH_4 \longrightarrow CH_3Br + H\cdot$$

$$I^{*} + CH_4 \longrightarrow CH_3I + H\cdot \quad .$$

The organic products are volatile and can be isolated from the irradiation cell by a sweeping technique similar to that used by Ockenden (68) for rare-gas studies.

The kinetic energy of fission recoils is very high compared to that of neutron-activated species (see Table VIII). It is unlikely, however, that this would have altered the nature of the hot-atom reactions as they would not be expected to occur until the recoil energy had dropped to about 5 electron volts.

The main difference between the fission-recoil and neutron activated species is that fragment ranges must be considered in the fission-recoil system. Ranges are of the order of two centimeters in gases at atmospheric pressure; some typical ranges are shown in Table

TABLE IX

Mean Ranges of U^{235} Fission Fragments in Various Gases*

	Air (mm)	H_2 (mm)	He (mm)	Ar (mm)	Xe (mm)
Light Fragment	25.4	21.1	28	23.9	23
Heavy Fragment	19.5	17.7	23	19.4	18

* Air data Bøggild (70), other gases Bøggild (71).

IX. The efficiency of the hot-atom reaction will be a function of the geometry of the system. The highest efficiency occurs in a system the dimensions of which exceed the fragment ranges.

Denschlag et al (66,67) have studied the reaction of fission recoils with methane. Separating the products by gas chromatography they found methyl and ethyl iodides in comparable quantities (69). The low yield prevented a more accurate assessment of the relative abundances.

A competing process would be the hot-atom reaction of secondary fission-product halogens with methane. As a result of the beta decay of its precursor, sufficient kinetic energy can be given to a halogen* to enable it to undergo hot-atom reactions similar to those of the fission-recoil fragments. Denschlag et al (66,67) have shown this process to be less favourable than that with the fission recoils.

Little interference would be expected from thermalized halogen atoms. Many will be lost by reactions with the walls; the rest will react with methane abstracting hydrogen:

$$Br + CH_4 \longrightarrow CH_3\cdot + HBr$$

$$I + CH_4 \longrightarrow CH_3\cdot + HI \quad .$$

The hydrogen halide will be lost by subsequent reaction with the walls.

---

*The recoil energies given to nuclei of masses 87 and 137 as a result of radioactive decay are shown in Appendix I.

b. Construction of Cell

The design of the irradiation cell is shown in Fig. 3. All construction was of 65S-T aluminum, with the exception of the target plates which were made of pure aluminum. The cell and its shutter (shown in Fig. 7) were made to fit through a 5.70 cm I.D. beam tube located in the beam port described in the next section of this chapter.

The target assembly consisted of a number of target plates and a number of spacers which positioned these plates. Photographs of the plates and spacers are shown in Figs. 4 and 5 respectively. One inner spacer and one outer spacer are shown inside the irradiation cell in Fig. 6. The target plates were made in two sizes which alternated to provide the gas-flow pattern shown in Fig. 3.

The target plates were coated with uranium oxide on both surfaces, with the exception of the end target plates which were coated only on their inner surfaces. The active volume of the cell was that contained between the inner surfaces of the two end target plates. The gas space between the target plates could be varied by the choice of the number and size of spacers used.

The target plate-and-spacer assembly was held in position by an end plate and its retaining ring. Adjusting screws on the end plate and retaining ring held the target plates and spacers firmly in place. A rounded end fitted over the end of the cell to operate the shutter.

A cadmium-covered shutter, shown in Fig. 7, was used to turn the neutron beam on and off. This shutter was a more rugged model of that described by Ockenden (68). Its operation can be seen in the sequence

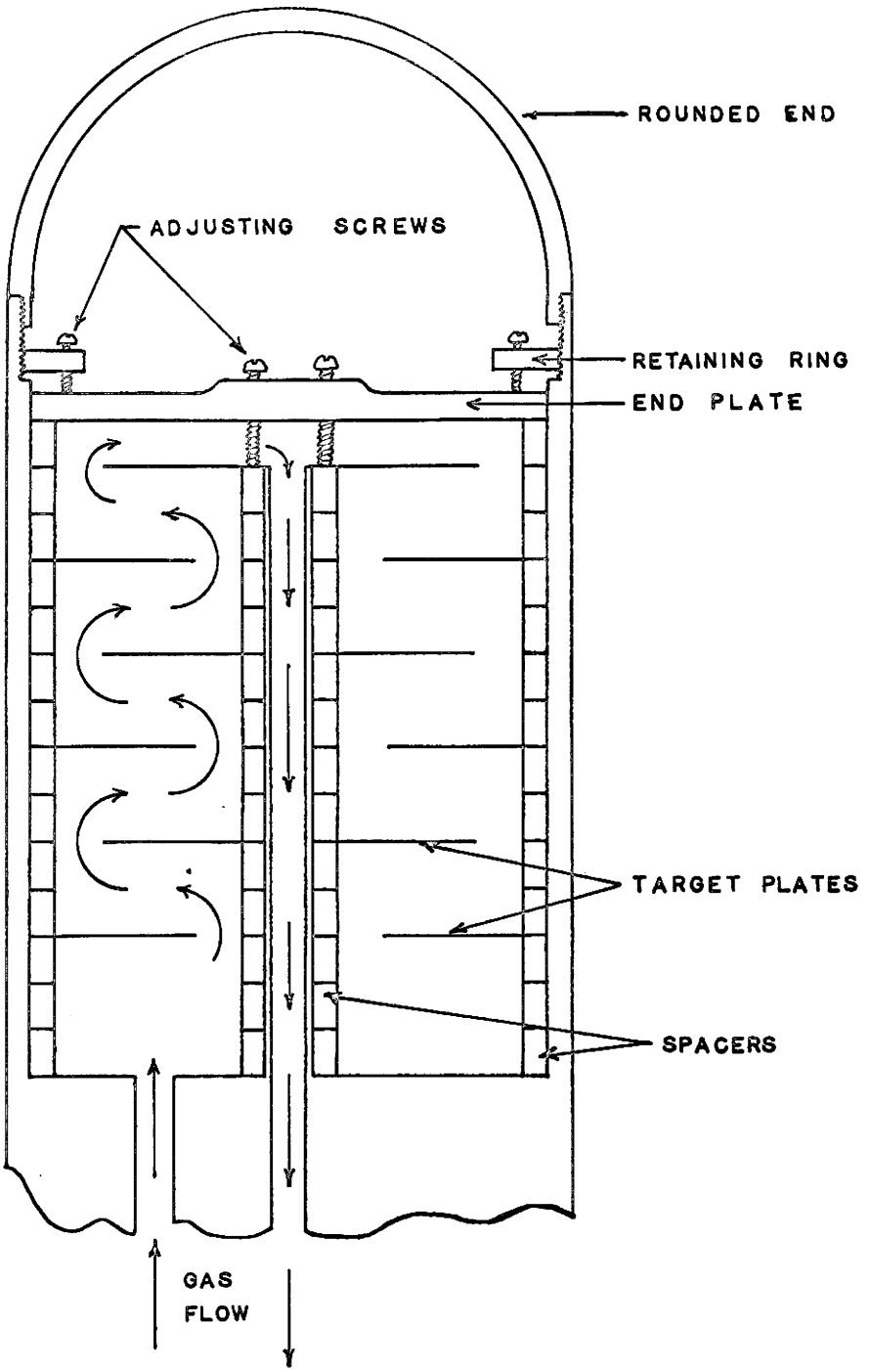

Fig. 3 CROSS SECTION OF IRRADIATION CELL

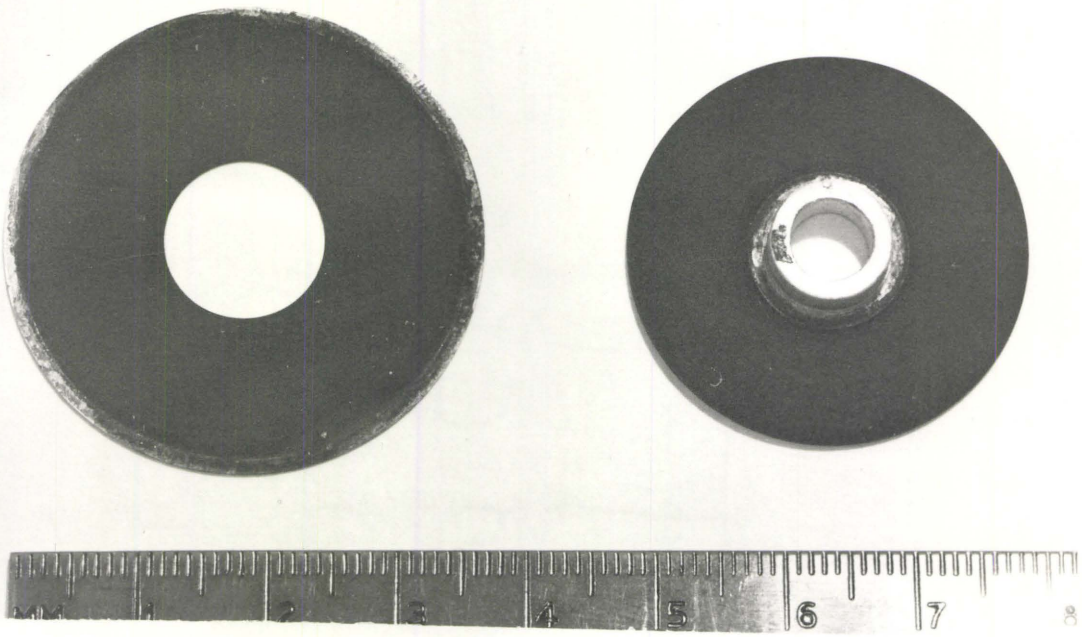

FIG. 4 URANIUM TARGET PLATES

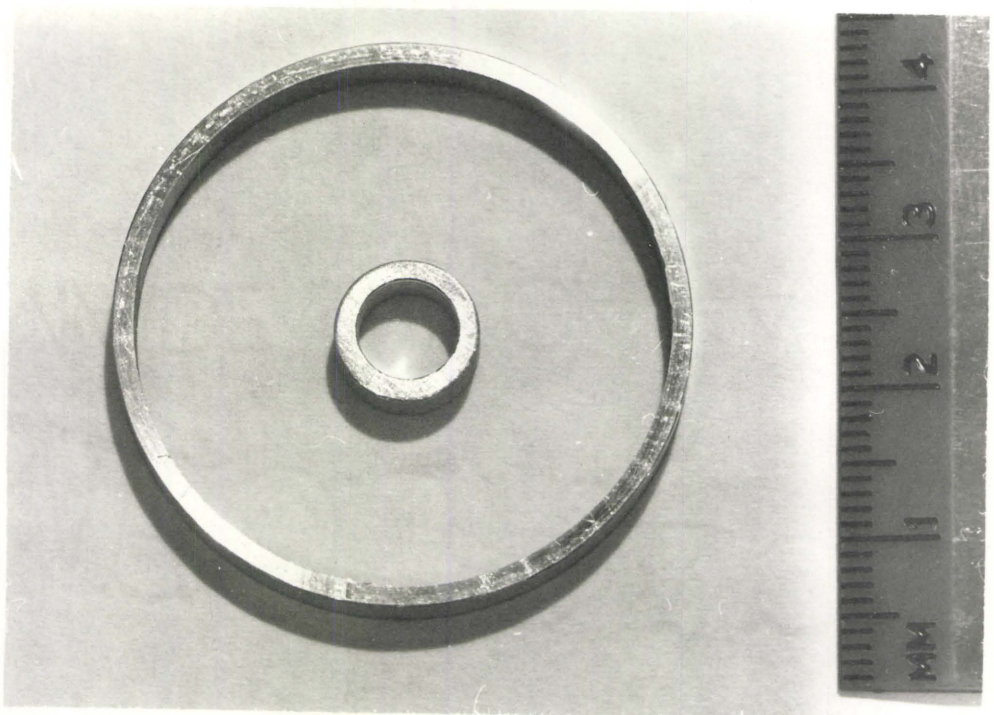

FIG. 5 SPACERS

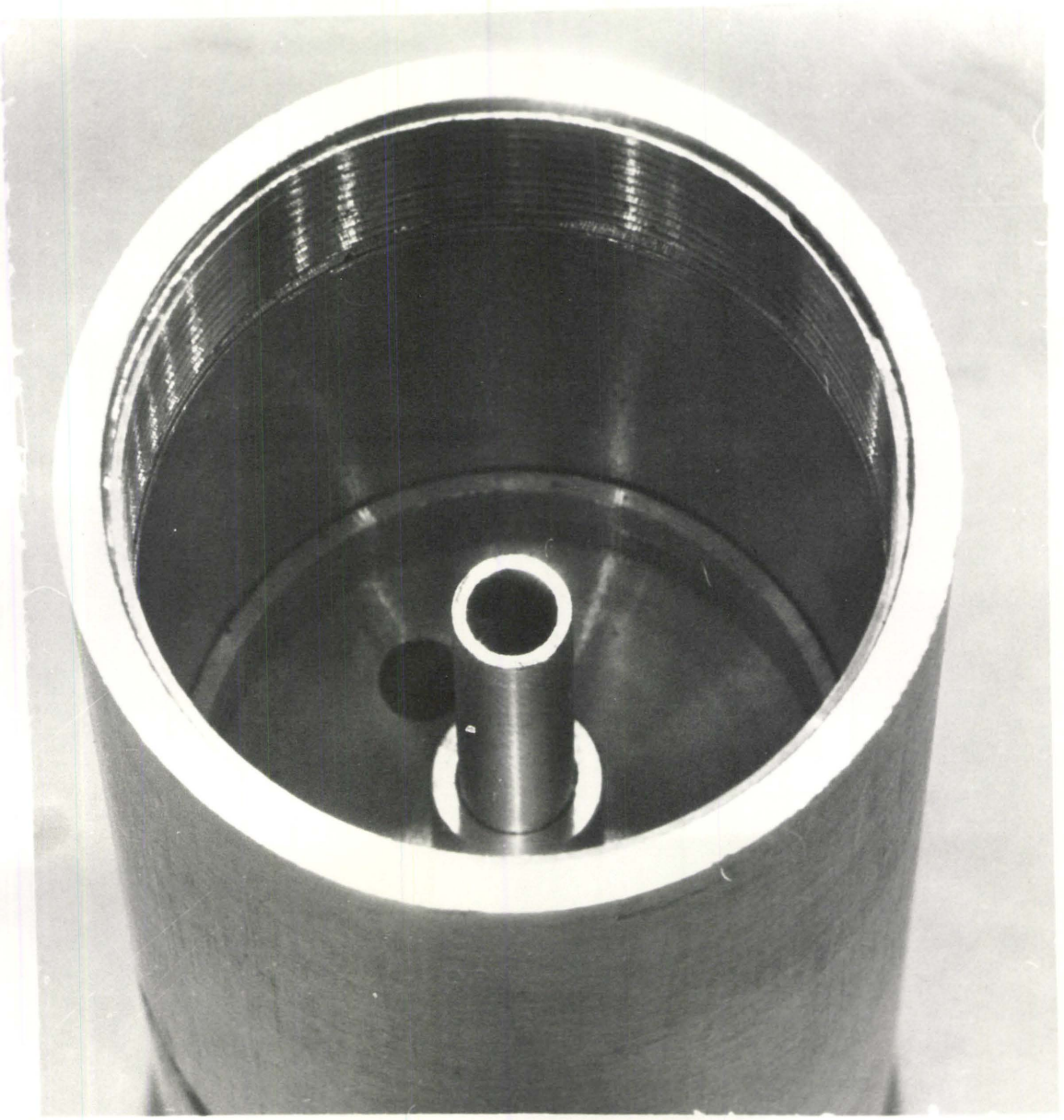

FIG. 6 IRRADIATION CELL

INSIDE VIEW

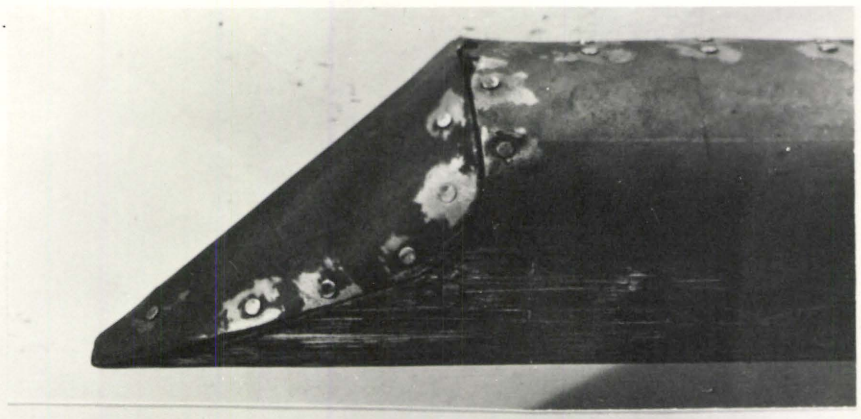

FIG. 7a MECHANICAL SHUTTER - CLOSED

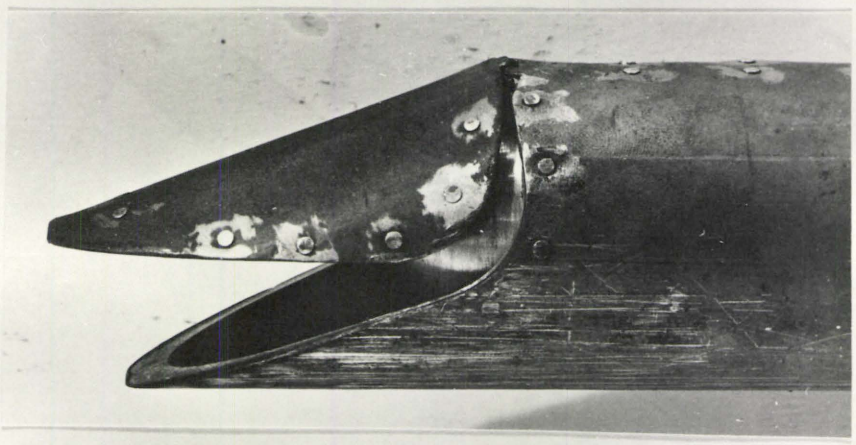

FIG. 7b MECHANICAL SHUTTER - PARTIALLY OPEN

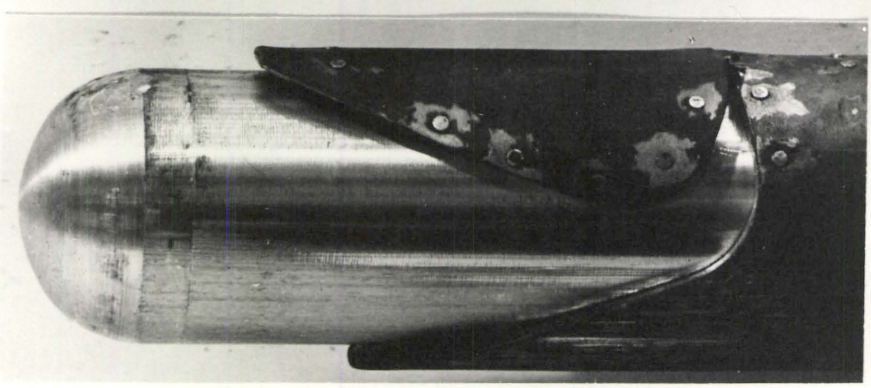

FIG. 7c MECHANICAL SHUTTER - OPEN

of photographs shown in Fig. 7.

The upper photograph shows the shutter pushed forward to its closed position. The front flap has dropped covering the irradiation cell with cadmium and thereby cutting off the neutron beam. The shutter when in this closed position attenuated the fission rate by a factor of 30.

The centre photograph shows the shutter being opened. It is being pulled back; the rounded end of the irradiation cell acting like a ramp lifts the front flap and exposes the cell to the neutron beam.

The lower photograph shows the shutter fully open. It has been pulled all the way back, exposing the cell to the neutron beam.

The neutron beam was "turned on and off" by moving the shutter back and forth between its two limiting positions (Fig. 7a and 7c). This was accomplished by means of the pneumatic shutter drive which was described by Ockenden (68) and has been adapted to this apparatus.

The cell and shutter were mounted at the end of a 3.5 metre length of 5.08 cm O.D. tubing which contained in its length paraffin and lead plugs for neutron and gamma shielding respectively. The leads for the gas-flow and shutter-drive systems passed through this shielding following a helical path which prevented any direct-line paths for escape of radiation. The pneumatic shutter drive was located at the outside end and was connected to the shutter by a flexible cable. The gas leads connected to an external gas-flow system by means of Swagelok "Quick-Connect" fittings. The complete apparatus which enabled handling and operation of the irradiation cell and its shutter is shown in Fig. 8.

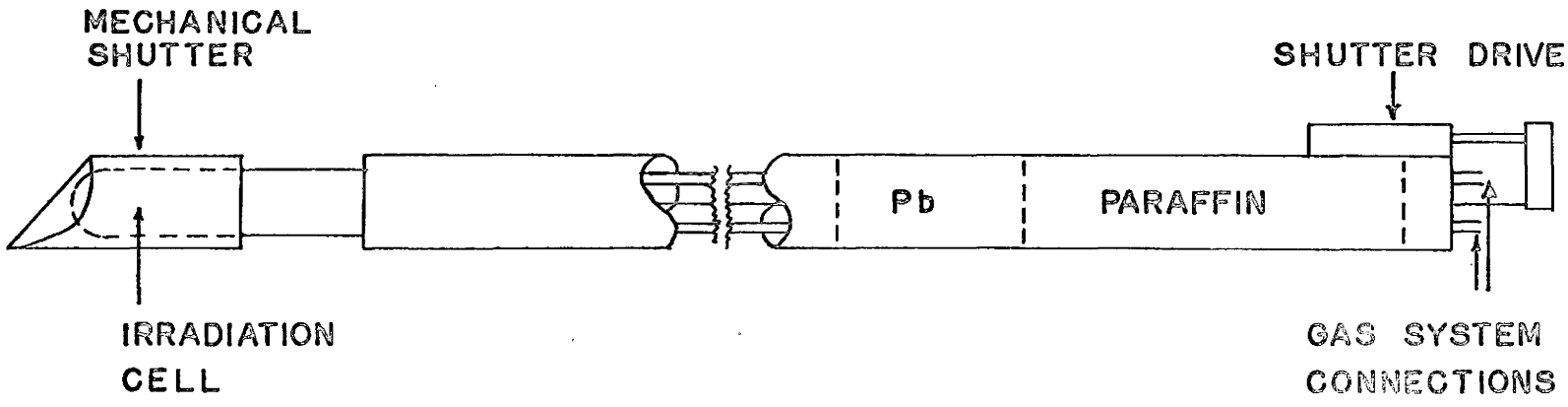

Fig . 8 IRRADIATION APPARATUS

c. Preparation of Target Plates

The target plates were constructed of pure aluminum 0.025 mm thick. The plates are shown in Fig. 4. The surfaces were anodized in order to retain a coating. The anodizing procedure was that used by Hallam (72); a potential of 150 volts was used, giving a thickness of 2000Å to the oxide coating.

Uranyl nitrate was painted by layers on to the surfaces from a dilute alcoholic solution containing a few percent polyethylene glycol (Carbowax 1500). Each layer was dried under an infra red lamp, then slowly heated above 350°C in order to convert the nitrate to the oxide. This process was repeated many times to obtain a sufficiently thick coating.

The low neutron flux in the beam port ($\sim 10^{10}$ n/cm^2/sec.) necessitated making a very thick coating of the oxide in order to get sufficient activity. The final coatings had thicknesses of four milligrams of U^{235} (93%) or U^{233} (100%) per square centimetre.

The polyethylene glycol acted as a wetting agent which spread the solution into uniformly thick layers. When heated, it decomposed to form a tarry substance which acted as a binder holding the uranium oxide together.

In use, the plates were very resistant to radiation and mechanical damage. Observation of the plates after a full year's operation showed no visible change in appearance or other properties.

d. Gas-Handling System

A schematic diagram of the gas-handling system is shown in Fig. 9. The system connected to the irradiation cell through Swagelok "Quick-Connect" Fittings S. The pressure of the system was set by the regulating valve* V1 on the gas cylinder. The flow rate of the sweeping gas was controlled by the needle valve V3 and the pressure drop across the system; the flow rate was observed on the flowmeter.

Valves V2, V4, V5 and V7 were toggle valves; V6 was a four-way stopcock. Traps T1 and T2 were reactive traps which isolated the halogen activity; they will be described in a subsequent chapter. T3 was a cold trap which stopped the rare-gas activities preventing their escape into the reactor exhaust system.

The gas-handling system was operated in the following four modes during an irradiation cycle:

Flush Cell: Valves V2, V4 and V7 were open, V5 was closed and V6 was set to by-pass the traps. In this mode the contents of the irradiation cell were swept directly into the cold trap removing any residual activity from the cell.

Irradiate: Valve V2 was open and the others were closed. The gas in the system was maintained at the pressure set by the regulating valve V1.

---

* Matheson two-stage regulating valve, calibrated with a mercury manometer.

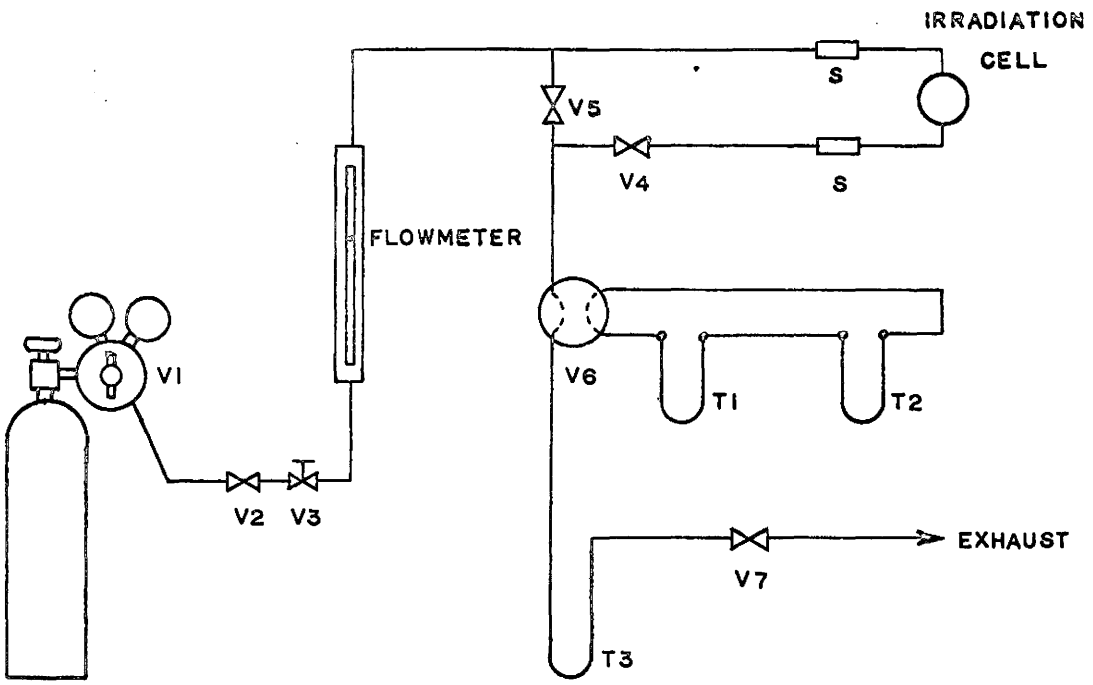

Fig. 9 GAS-HANDLING SYSTEM

V1 – REGULATING VALVE
V2,4,5,7 - TOGGLE VALVES
V3 – NEEDLE VALVE
V6 – FOUR-WAY STOPCOCK
T1,2,3 – TRAPS
S – SWAGELOCK "QUICK-CONNECT"

Sweep: Valves V2, V4 and V7 were open, V5 was closed and V6 was directed through traps T1 and T2. The sweeping gas swept the activity from the cell through the traps.
The halogen activity stopped in Traps T1 and T2 and the rare gas activity stopped in Trap T3.

Flush Traps: Valves V2, V5 and V7 were open, V4 was closed and V6 was directed through traps T1 and T2. A flow of clean gas swept through the traps removing residual activity from line.

The methane which was used as the reaction medium was also used as a carrier gas for sweeping the cell. This eliminated the need of a more complex gas-handling system.

(ii) Beam Port

The experiments were carried out in "No. 2 Beam Port" of the McMaster Nuclear Reactor. The beam port design has previously been described (68,73) and is shown in Fig. 10.

The high gamma-radiation field from the reactor core was kept to a minimum by plugs of graphite* and bismuth which reduced the field by many orders of magnitude. The plugs may be seen in the photograph shown in Fig. 11. The neutron and gamma beams were collimated by a stepped

---

* Graphite was used to reduce the gamma field by an order of magnitude before reaching the bismuth plugs; this eliminated the need for forced cooling of the bismith plug.

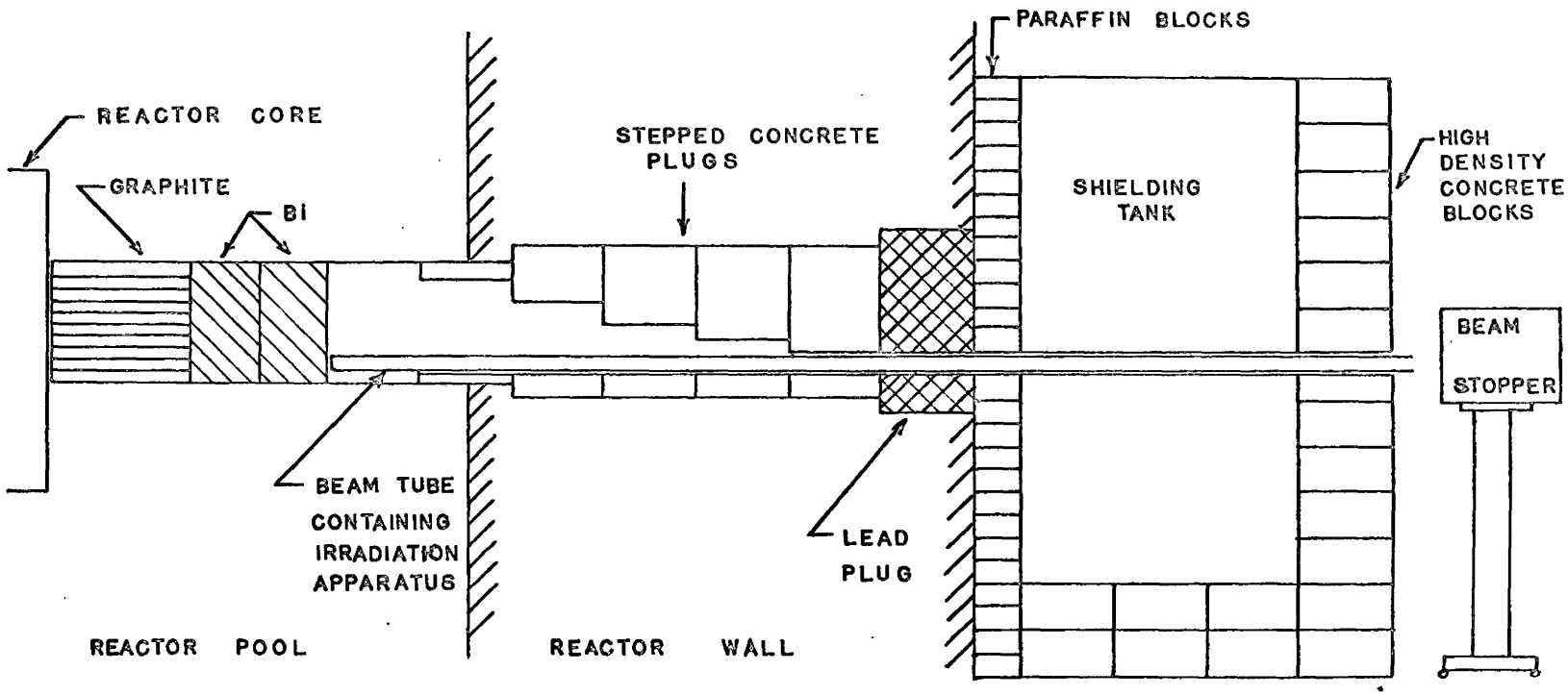

Fig. 10 BEAM PORT No. 2 McMASTER NUCLEAR REACTOR

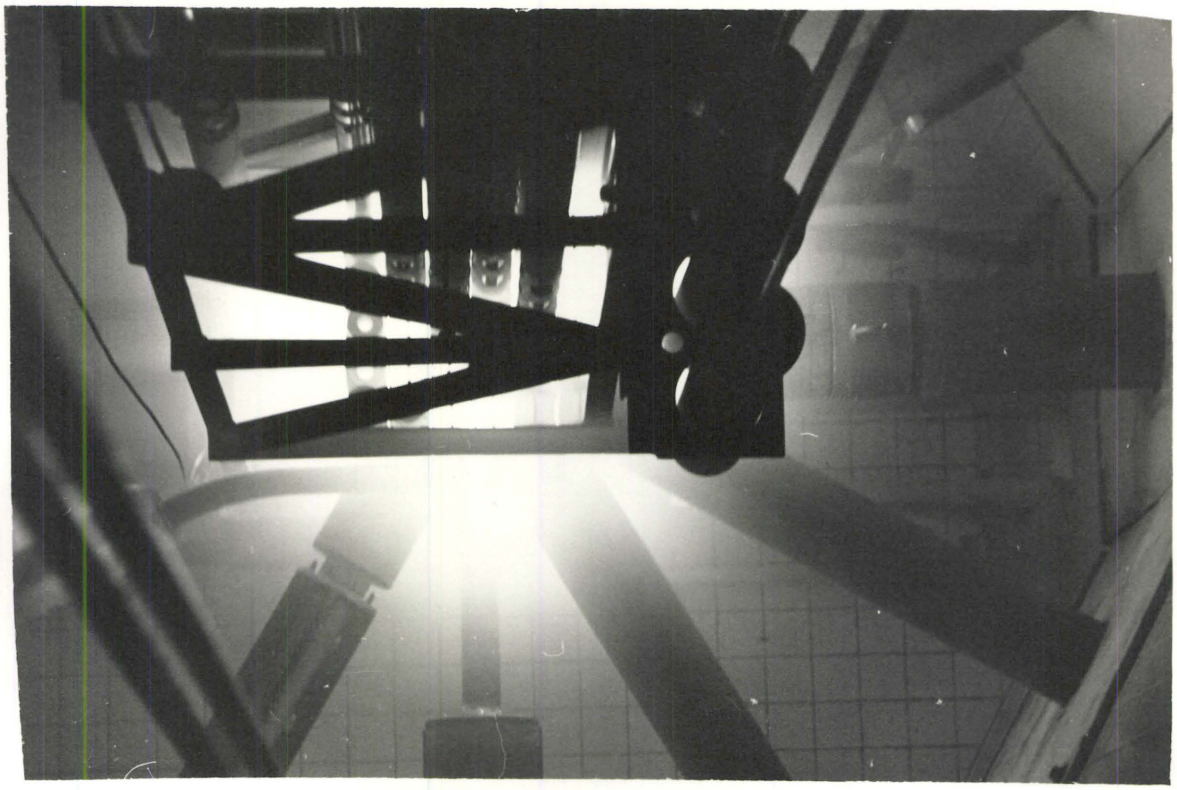

FIG. 11 BEAM PORTS

McMASTER NUCLEAR REACTOR

The photograph shows the beam ports of the McMaster Nuclear Reactor. Beam Port No. 2 extends from the right-hand side of the reactor core through the wall at the right of the photograph. The photograph shows the graphite and bismuth plugs as well as the table supporting them.

TABLE X

Thermal-Neutron Fluxes in Beam Port*

Position (Distance from Core End	Relative Flux	Actual Flux
0 cm.	160	5×10^9 n/cm^2/sec
30	23	7×10^8
60	13	4×10^8
90	4.1	1×10^8
120	2.3	7×10^7
150	1.4	4×10^7
180	1.0	3×10^7
Core		1.4×10^{13}

* Measurement made December 1960 by activation of Mn^{55}
Reactor Power Level - one megawatt

series of high-density concrete plugs and a lead plug before they left the reactor wall. Scattered neutrons were stopped outside the wall by a 950 litre tank of a dilute solution of boric acid. This tank was surrounded by high-density bricks which stopped scattered gamma radiation.

The beam tube, a capped aluminum tube, was used to contain the irradiation apparatus, described in the previous section of this chapter, with the irradiation cell at the core end and the gas connections at the wall end. The beam tube could also be used with the irradiation apparatus used by Ockenden (68) and a low temperature apparatus (72). The three systems could be interchanged rapidly.

Radiation streaming through the beam tube was stopped by a moveable beam stopper. With the reactor operating at a 2 MW power level, the radiation field was well below health tolerances at all points around the beam port.

The neutron fluxes measured at various positions inside the beam tube are shown in Table X.

(iii) Counting Techniques

a. Neutron Detection

Neutron detection was carried out using a Texas Nuclear Corporation Model 325, TEXLIUM detector. This detector was a proportional counter filled with helium-3 gas to a pressure of ten atmospheres. This design of counter has been described by Batchelor (16) and is based on the reaction:

$$He^3 + n \longrightarrow H^3 + p + 764 \text{ keV.}$$

The detector measures the total energy of the proton and triton giving a pulse proportional to the energy of the incident neutron plus 764 keV the Q of the reaction. The pulse-height distribution obtained from thermal neutrons is shown in Fig. 12.

The efficiency of the detector is proportional to the capture cross section, σ_p, for the (n,p) reaction. At thermal energies σ_p has a value of 5500 barns (74). It drops to one barn in the region 100 keV to 2 MeV, which is the energy range of the delayed neutrons from fission. Therefore the sensitivity for delayed neutrons is three orders of magnitude lower than for thermal neutrons.

In order to increase the sensitivity for delayed-neutron detection, the detector was imbedded in paraffin wax which served to moderate the fast neutrons to thermal energies; thereby, putting them into the energy region to which the detector is most sensitive. It was assumed that the response was adequately linear with energy in the energy region of delayed-neutron emission. This assumption seemed valid as the delayed-neutron groups fall into the same energy regions (see Table II).

The detector's neutron background was kept to a minimum by use of a cadmium and paraffin-wax shield which surrounded the detector and its moderator. Using the shield, a background of 0.5 counts per second was obtained with the reactor operating at a power level of 2 MW.

A block diagram showing the neutron-detection system is shown in Fig. 13. The high voltage was supplied from four three-hundred volt batteries connected in series. With the very small pulses produced by the detector (5 mv. negative with a 2 microsecond rise time) the battery supp-

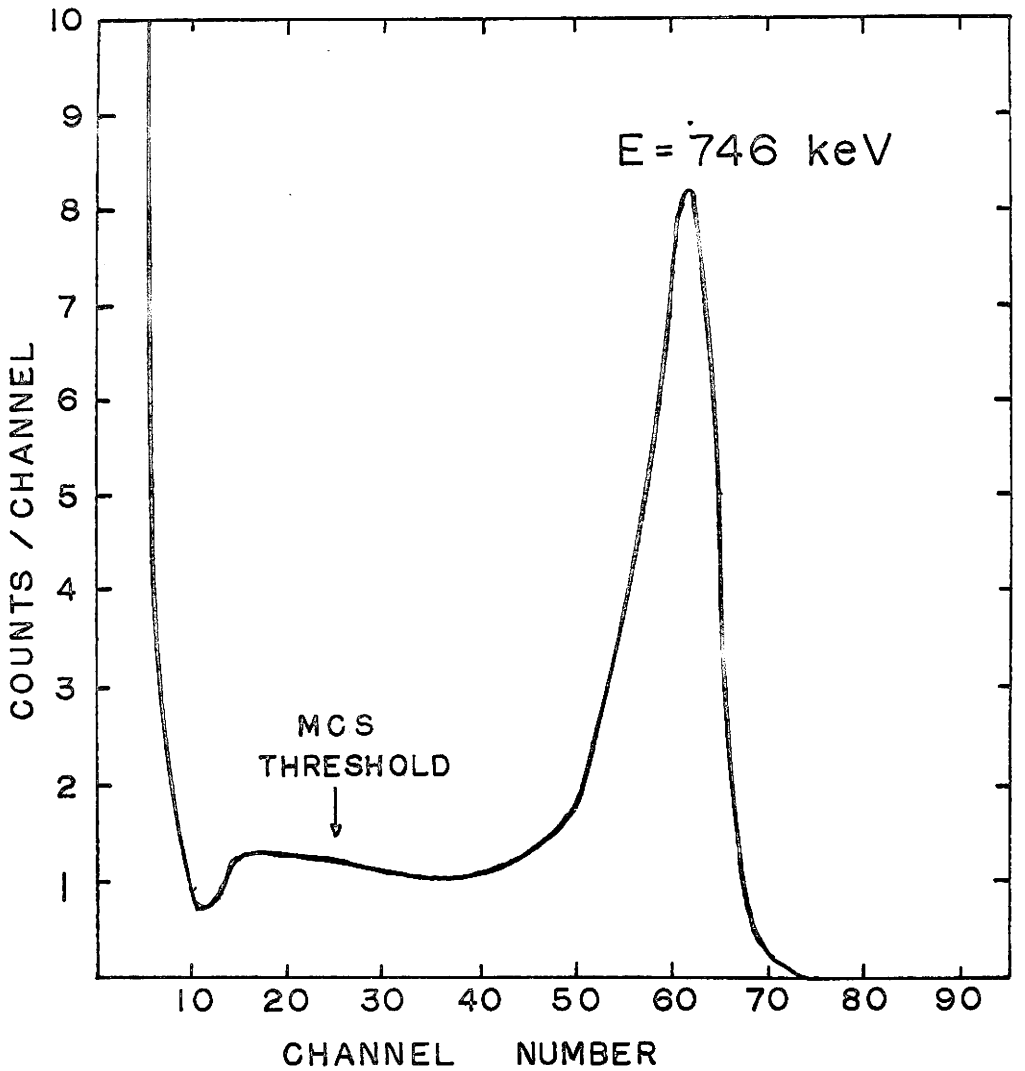

Fig. 12 PULSE-HEIGHT RESPONSE OF He^3 DETECTOR TO THERMAL NEUTRONS

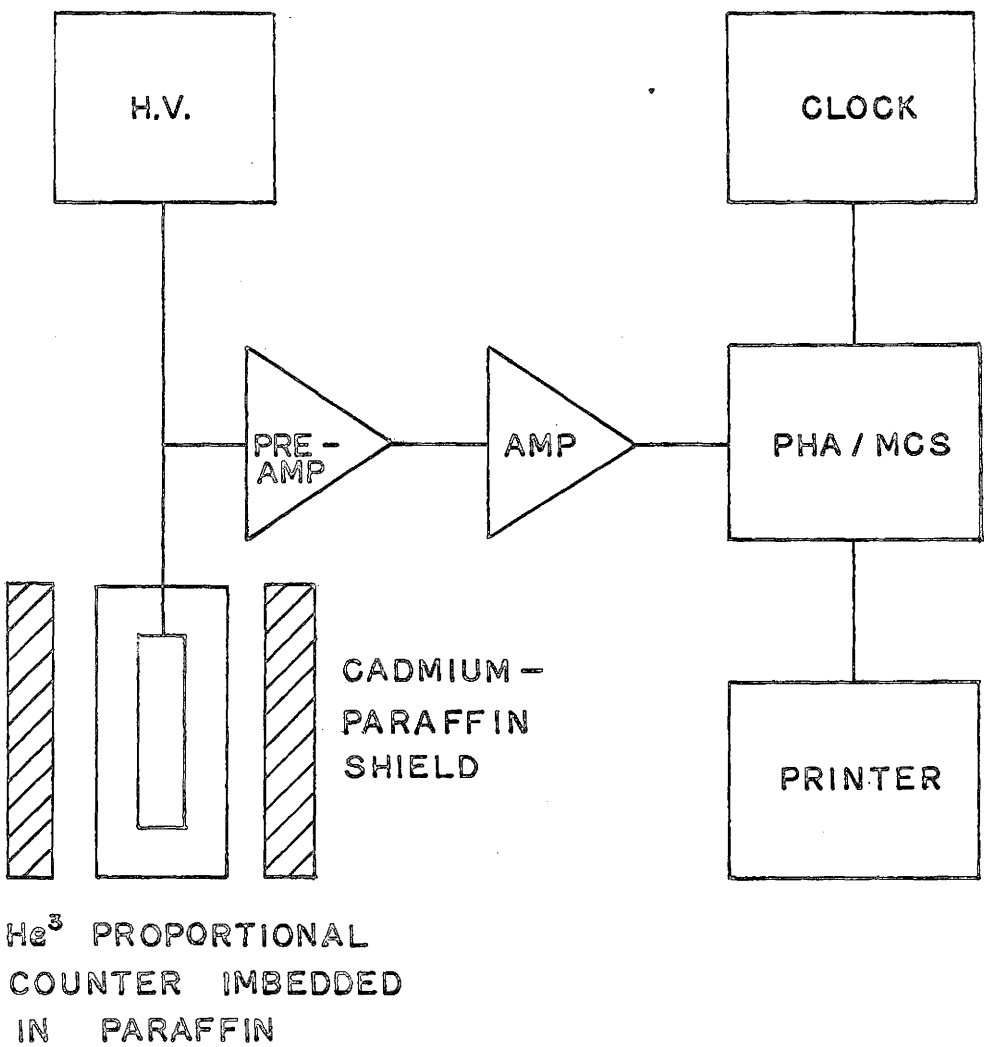

Fig. 13 BLOCK DIAGRAM OF NEUTRON COUNTING SYSTEM

ly was found to be more suitable than a regulated supply due to the lower noise level of the former.

The detector's output pulses were fed into a Baird Atomic (model 219A) preamplifier (gain of twenty) and a Radiation Counter Laboratories (model A-61) linear amplifier. The output of the amplifier was fed into a Nuclear Data (model 101) multi-channel analyzer.

The analyzer was modified to operate as a multi-channel scaler; the address scaler being advanced by an external clock constructed from a Baird Atomic Industrial Glow Tube Counter. The clock counted the sixty cycle line frequency and fed the output of its last Dekatron tube into a Schmidt trigger which produced the correct-shaped address-advance pulses.

In order to reduce the system's sensitivity to beta and gamma radiation, the multi-channel scaling threshold was set at 300 keV; thus, pulses lower than 300 keV were rejected. A one centimetre lead shield between the source and the detector minimized betas and low-energy gammas. It is unlikely that high-energy gammas would deposit sufficient energy in the detector to be counted. In a gamma field exceeding 2R/hr., no counts were recorded above the neutron background.

b. Gamma-Ray Detection

Gamma radiation was detected using a Harshaw 3" x 3" thallium-activated sodium iodide crystal integrally mounted to a Dumont 6363 photomultiplier. The resolution of the crystal was 8.2% for the 662 keV gamma ray of Cs^{137}. The output of the photomultiplier was fed through a cathode follower to the Radiation Counter Laboratory amplifier and the Nuclear Data analyzer.

The high beta-decay energies of the short-lived fission products necessitated rather thick beta absorbers in front of the crystal. A lucite absorber of thickness 3.0 gm/cm^2 was used in front of the crystal at all times.

(iv) Data Analysis

The decay curves obtained from the decay of the delayed-neutron activity were analyzed using the computer program MADCAP* and the IBM 7040 computer at McMaster University. Computer analysis has the advantage of providing the "best" fit to the data, speed, and removal of the human subjectivity of graphical methods.

MADCAP is a least-squares regression program written in Fortran IV and is a modification of a program written by Archer (75). MADCAP could be operated in either of two modes for determination of intensities or half-lives

Intensities: The half-lives for all the components are known; the intensities of both parent and daughter isotopes contributing to the decay are to be determined. MADCAP generated a decay curve for each component; these curves were fitted to the data by the method of linear least- squares.

Half-Lives: The half-lives of one or more of the components are unknown and to be determined. A non-linear least-squares regression was used to evaluate the half-lives. MADCAP was given a "guess"; it evaluated chi-squared, the goodness of fit, at this guessed value. The "guess" was incremented in small steps, evaluating chi-squared at each step. The

---

* MADCAP - Marvin Silbert Decay Curve Analyzing Program.

values of chi-squared were fitted to a parabola, the minimum of which corresponded to the "best" half- life for the component.

The intensities were evaluated in the same manner as before using the half-lives determined by MADCAP.

Subroutines, PEDRO and RATIO, subtracted background from the input data and determined the relative ratios of the intensities respectively.

CHAPTER IV

EXPERIMENTAL

(i) Preliminary Experiments with Neutron-Activated Bromine

As an introduction to this work, the hot-atom reactions of neutron-activated bromine were studied. These provided a familiarization with the hot-atom process. Hot Bromine was produced by the reactions:

$$Br^{79}\ (n,\gamma)\ Br^{80},\ Br^{80m}$$

$$Br^{81}\ (n,\gamma)\ Br^{82}$$

$$Br^{80m}\ (I.T.)\ Br^{80}$$

These reactions were studied in various liquid organic media. Their products were analyzed by gas-chromatographic techniques (64), using as a detector a gas-flow proportional counter. The gas chromatograph and its detector are shown in Figs. 14 and 15 respectively.

Fig. 2 shows a gas chromatogram of the radioactive products of the $Br^{81}(n,\gamma)\ Br^{82}$ reaction in liquid n-propylbromide, scavenged with elemental bromine. The chromatograms produced from the products of the three nuclear processes were indistinguishable; the product distribution being independent of the initial recoil energy.

(ii) Chemical Isolation of Fission-Recoil Bromine

The main chemical species, present in the irradiation cell, were methyl and higher halides (69) produced by hot-atom reaction of the halogens with methane. The halides were present along with the rare gases, krypton and xenon, dissolved in a methane gas stream.

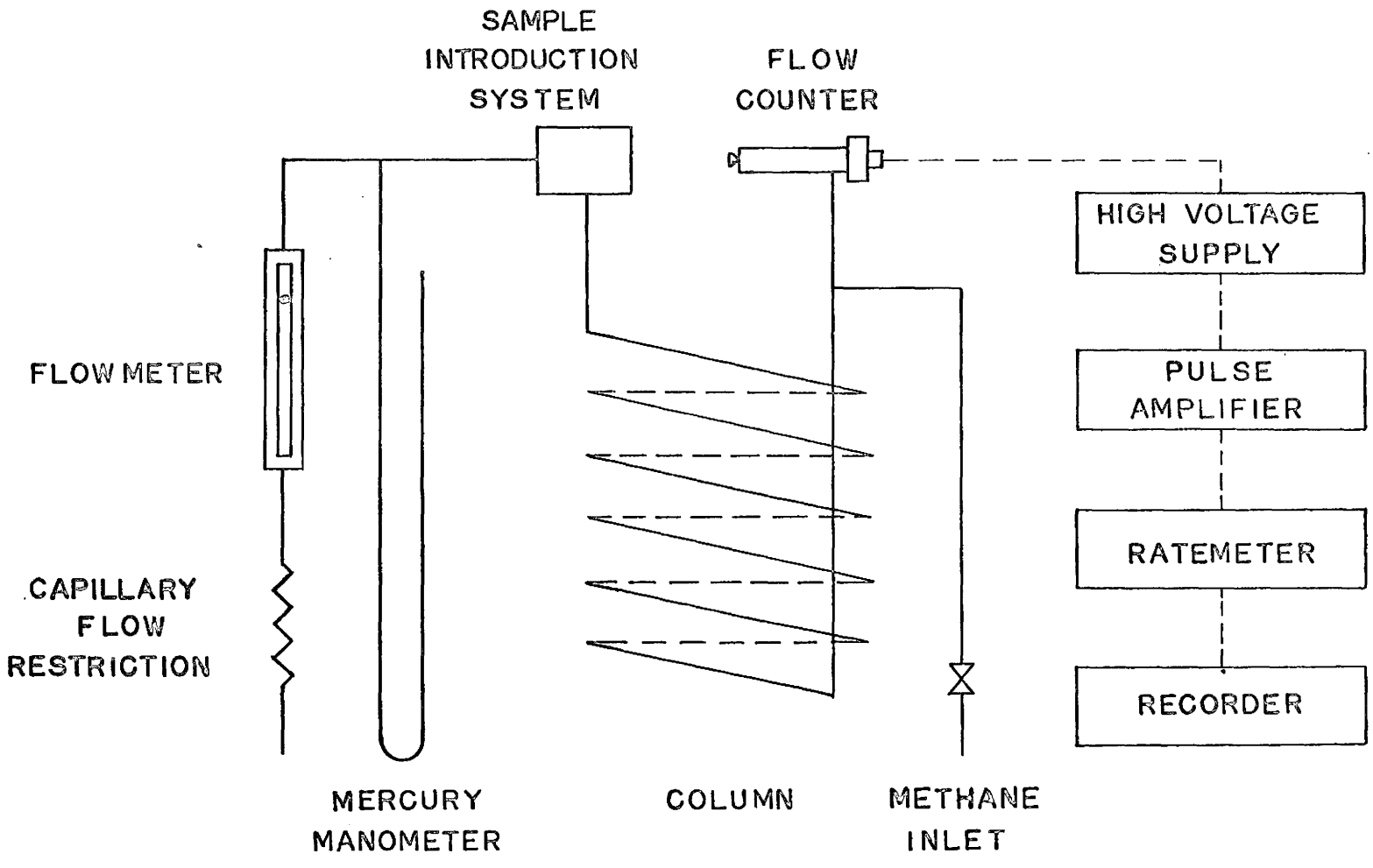

GAS - CHROMATOGRAPHIC APPARATUS

FIGURE 14

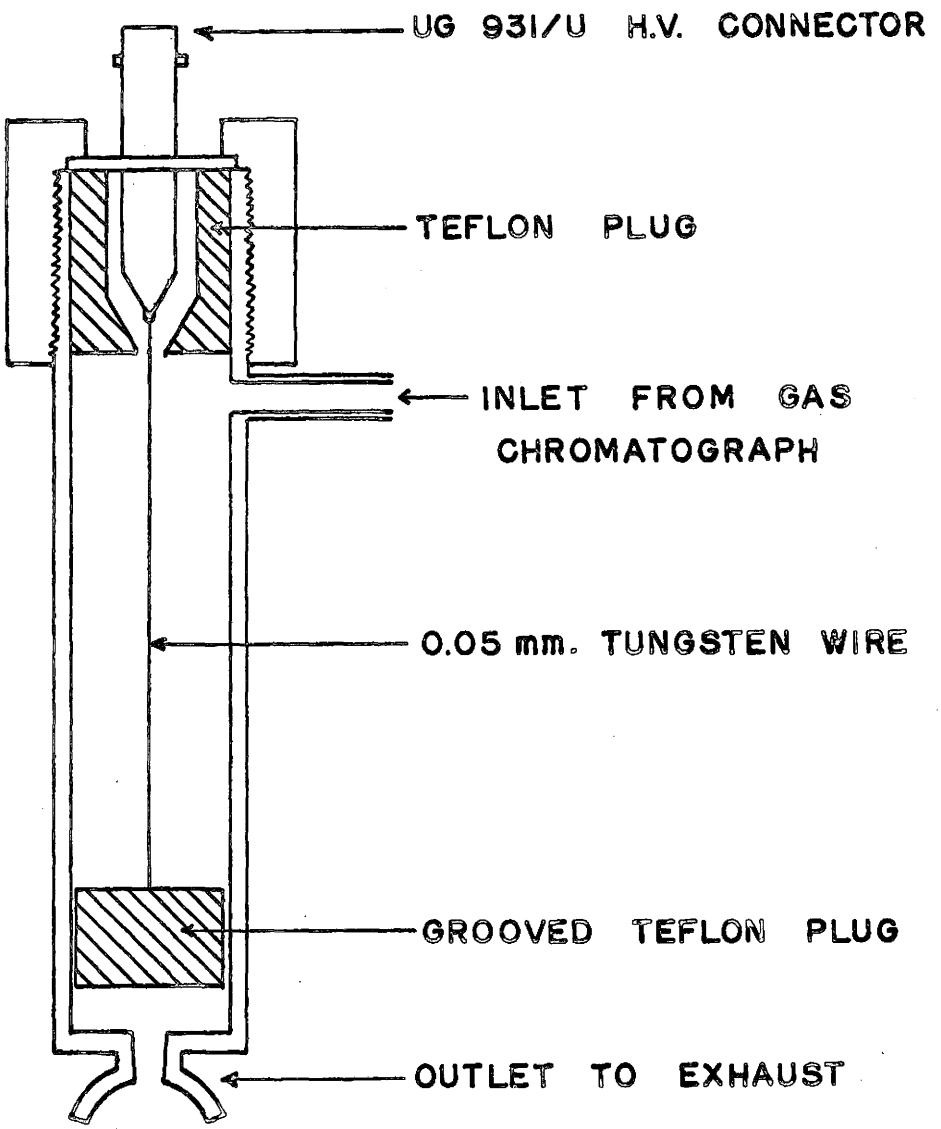

Fig. 15 CROSS SECTION OF FLOW COUNTER

Gas chromatography has been used successfully to separate the products of the hot-atom reactions of fission-product halogens (66,67). This method is too slow however for the separation of the short-lived bromine isotopes. Differences in physical properties, such as boiling points, are insufficient to be useful for the very rapid separations necessary with nuclides of very short half-lives. The boiling points of the various products, present in the irradiation cell, are shown in Table XI.

The separational techniques that were attempted were based upon differences in adsorption (molecular sieve), chemical reactivity, and rates of exchange. The traps (T1 and T2 in Fig. 9) were lengths of 8 mm. O.D. pyrex tubing filled with 2 to 3 cm. lengths of various adsorbing and reacting materials. The activity was brought from the cell to the traps using the procedure outlined in Table XII. The delayed-neutron activity was measured at the second trap and was analyzed for the presence of both iodine and bromine activities. The efficiency of the various traps used to collect the halogen activity is shown in Table XIII.

Experiment number 1 indicates the presence of materials, containing bromine and iodine, which are filterable by or reactive with glass wool. Experiment number 2 indicates that one glass wool trap is sufficient to remove these entirely from the gas stream. Subsequent experiments considered the isolation only of the bromine and iodine activities which passed through glass wool in trap No. 1.

TABLE XI

Boiling Points of Volatile Products Produced
By Hot-Atom Reaction of Fission Recoils with Methane

Element or Compound	Boiling Point (76)
Kr	-152.9°C
Xe	-107.1
CH_3Br	3.56
C_2H_5Br	38.0
CH_3I	42.5
C_2H_5I	72.2

TABLE XII

Irradiation Procedure

Time*	Operation
-15 sec. to t_o	Flush cell
t_o to t	Irradiate
t to t + 5 sec.	Sweep**
t + 5 to t + 10 sec.	Flush traps
t + 10 sec.	Start analyzer

* t_o and t refer to the start and end of the irradiation.

** Sweeping times as short as 2 seconds were also used.

TABLE XIII

Efficiency of Traps for Collection of Halogen Activity

Experiment Number	Trap No. 1	Trap No. 2	Approximate Delayed-Neutron Yield on Trap No. 2 *
1	-	Glass Wool	10^3
2	Glass Wool	Glass Wool	0
3	Glass Wool	Molecular Sieve 4A	10^2
4	Glass Wool	Molecular Sieve 5A	10^2
5	Glass Wool	Molecular Sieve 13X	10^3
6	Glass Wool	$AgNO_3$	10^2
7	Glass Wool	$AgNO_3$ (120°C)	10^3
8	Glass Wool	NaI (25°C)	0
9	Glass Wool	NaBr (25°C)	0
10	Glass Wool	NaI (200°C)	0
11	Glass Wool	NaBr (200°C)	0

* Includes both Bromine and Iodine activities, which were both present in all samples.

Molecular sieves* with their structure of caves and caverns have the ability to "trap" molecules of one size, while passing those of other sizes. Molecular sieve adsorption has been used in gas chromatography(77) to selectively trap organic materials from gas streams. It was hoped that a difference in sizes of the organic halides could lead to a separation by molecular sieve adsorption.

Experiments numbers 3, 4 and 5 (Table XIII) show the results of passing organic halides through traps filled with various molecular sieves. The 4A and 5A molecular sieves were not as efficient as was the 13X molecular sieve. All three molecular sieves trapped an activity which contained both bromine and iodine in comparable quantities.

Silver nitrate has been used successfully as a reactive gas-chromatographic precolumn trap by Harris (78) to remove more reactive bromides from the simpler primary bromides. The removal was based upon loss of the bromide by reaction with the silver nitrate. The organic iodides being much more reactive than the corresponding bromines, it was hoped that they could be separated from the bromides by their reaction with silver nitrate**.

Experiment number 6 (Table XIII) showed that iodide activity was stopped on the silver nitrate. The iodide activity was, however, accompanied by a comparable quantity of bromine activity. Increasing the temperature of the trap (experiment number 7) increased the yield of halogen activity on the silver nitrate trap.

---

* Molecular sieves were from Linde Air Products. The designations 4A, 5A and 13X refer to their effective pore diameters (in Å).

** The silver nitrate was coated 50% by weight on C-22 Firebrick.

Attempts to exchange the halogens of the organic halides, with ionic halide salts (Experiments 8-11, Table XIII) were unsuccessful. The flow rate (1.5 to 2 litres/min.) was probably too fast to allow sufficient time for any exchange to occur.

Both the 13X molecular sieve and the hot silver nitrate stopped the halogen activity with high efficiency. No further halogen activity was found in the cold trap leading to the exhaust system. Neither of the two traps was, however, able to distinguish between bromine and iodine. In order to differentiate between the two halogens, various traps were used ahead of trap No. 2 which contained either 13X molecular sieve or hot silver nitrate. These traps all contained glass wool to remove filterable activity. Table XIV shows the results obtained.

Experiments numbers 1 to 6 (Table XIV) used molecular sieve pretraps. The 4A and 5A molecular sieves had little or no effect upon the iodine content; it was present in quantities comparable to those of bromine. The 13X molecular sieve removed all halogen activity. None got to Trap No. 2.

The use of silver nitrate is seen in experiments 7 to 12 (Table XIV). Silver nitrate reduced the iodine content considerably. Heating the silver nitrate, however, stopped all of the halogen activity. A small concentration of iodine, ~10%, was evident from the presence of a long lived activity in the traps. Two gamma-ray peaks at 530 and 364 keV were identified as I^{133} and I^{131} respectively (79). Increasing the size of the silver nitrate trap from 3 cm. x 8 mm. O.D. to 25 cm. x 25 mm. O.D. removed all traces of the iodine activity.

This large silver nitrate trap was used in all subsequent experiments discussed in this work. Its large quantity of silver nitrate reacted

TABLE XIV

Collection of Bromine Activity, Free of Iodine

Experiment Number	Trap No. 1	Trap No. 2	Iodine Content Relative to Bromine *
1	Molecular Sieve 4A	Molecular Sieve 13X	comparable
2	Molecular Sieve 5A	Molecular Sieve 13X	comparable
3	Molecular Sieve 13X	Molecular Sieve 13X	-
4	Molecular Sieve 4A	$AgNO_3$ (120°C)	comparable
5	Molecular Sieve 5A	$AgNO_3$ (120°C)	comparable
6	Molecular Sieve 13X	$AgNO_3$ (120°C)	-
7	$AgNO_3$ (25°) Small	Molecular Sieve 13X	~10%
8	$AgNO_3$ (120°) Small	Molecular Sieve 13X	-
9	$AgNO_3$ (25°) Large	Molecular Sieve 13X	none detected
10	$AgNO_3$ (25°) Small	$AgNO_3$ (120°)	~10%
11	$AgNO_3$ (120°) Small	$AgNO_3$ (120°)	-
12	$AgNO_3$ (25°) Large	$AgNO_3$ (120°)	none detected

* Comparable indicates that bromine and iodine were present in approximately equal quantities.

The dash indicates that no halogen activity was present on Trap No. 2.

TABLE XV

Half-Lives of Bromine Delayed-Neutron Activities*

Author	Br^{87}	Br^{88}	Br^{89}
Snell (20)	54 ± 1		
Sugarman (80)	56.1 ± 0.7	15.5 ± 0.3	
Keepin (10)	54.5 ± 0.9		
Perlow (21)		15.5 ± 0.4	
Perlow (22)		16.3 ± 0.8	4.4 ± 0.5
Williams (31)	55.4 ± 0.7		
This Work	55.8 ± 0.5	15.9 ± 0.2	4.5 ± 0.8

* Uncertainties are ± 2σ

completely with the organic iodides, removing them from the gas stream while its glass wool filter removed any filterable material. Heating of this trap to 50°C prevented condensation of organic material on its surface. This temperature was not high enough to cause any appreciable reaction with the bromides. The 13X molecular sieve was generally used following the silver nitrate trap as it had the advantage of not requiring heating.

The rare-gas activity passed through both traps and stopped in the cold trap. The cold trap was filled with charcoal and was cooled with dry-ice and alcohol (liquid air could not be used as a coolant as it would also condense methane).

The half-lives of the bromine delayed-neutron precursors were obtained from the decay curves by use of the computer program MADCAP. The half-lives are shown in Table XV along with previously reported values. The values obtained are in good agreement with the previous values. A gamma spectrum of Br^{84} was obtained and corresponds with that reported by O'Kelly (81). No residual activity remained upon the decay of the Br^{84}.

(iii) Factors affecting yield of Organically-Bound Bromine

a. Addition of Inert Moderator

Hot-atom reactions can be differentiated from thermal-type reactions by the sensitivity of the former to the addition of inert moderators. If the reactions occurring in the irradiation cell are hot-atom rather than thermal, their yield will be reduced by the addition of inert moderators.

In order to confirm that the reactions used to isolate the bromine activity from the uranium were hot-atom in nature, the sweeping gas was alternated between methane and a gas mixture of 10 mole % methane and 90 mole % argon. The bromine yield was determined in each case. The average

values of the yields are shown in Table XVI.

TABLE XVI

Effect of Inert Moderator Upon Yield of Bromine

Gas	Yield of Bromine (Counts in 1st 10 channels)
100% CH_4	$6.1 \pm 0.2 \times 10^3$
90% Ar - 10% CH_4	$1.6 \pm 0.3 \times 10^3$

The results show a drop of a factor of four using the gas mixture. A similar drop was observed by Rack (59) in his studies with neutron activated bromine. The drop in yield confirms that the bromine is produced largely, if not completely, by a hot-atom process.

b. Length of Irradiation Time

The high radiation field inside the irradiation cell could give rise to radiation-induced reactions. If the irradiation were sufficiently long, a high concentration of radiolysis products could be built up. If their concentration were sufficiently high a significant portion of the hot-atom reactions could occur with the radiolysis products as well as with the methane. This would lead to a change in the yields of hot-atom products as the irradiation time increases.

In order to assess the contribution of radiation-induced reactions upon the total yield, determinations were made of the yield of bromine as a function of irradiation time. Fig. 16 shows the relative yields of the three bromine isotopes, Br^{87}, Br^{88} and Br^{89}, plotted as a function of irradiation time. The yields are compared with an "infinite" irradiation;

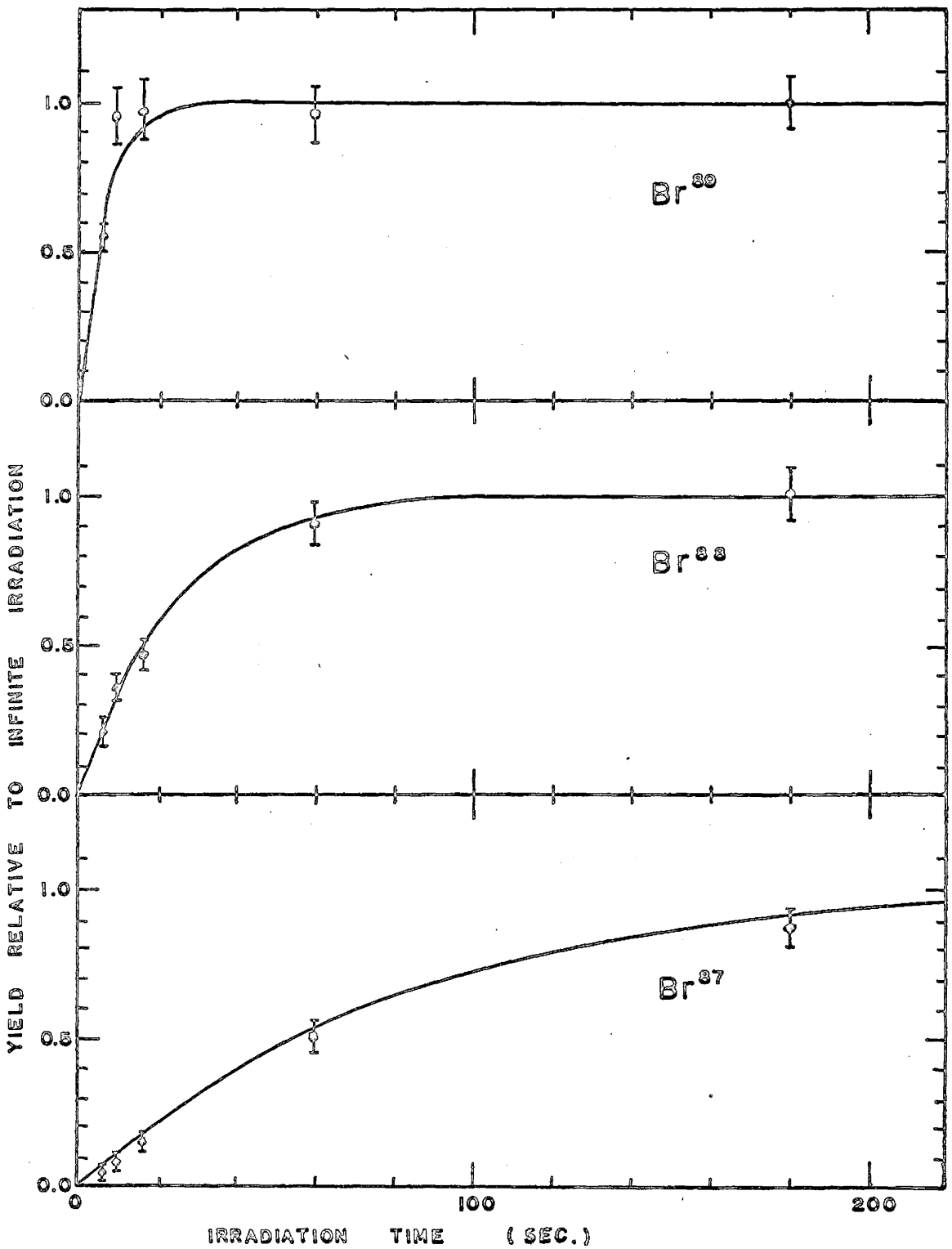

Fig. 16 YIELD VS IRRADIATION TIME

SOLID LINES REPRESENT $(1-e^{-\lambda t})$; POINTS ARE MEASURED VALUES

infinite being 480 seconds. The points are in agreement with the predicted rate of buildup with irradiation time, $(1 - e^{\lambda t})$. This agreement indicates that no significant long-term radiation-induced reactions were occurring during the irradiation.

c. Cell Pressure

As the pressure inside the irradiation cell increases, the yield of bromine would be expected to increase since the fraction of recoil fragments stopped in the gas increases. At sufficiently high pressures all of the fragments will be stopped in the gas and the yield will cease to rise with increasing pressure.

The yields of Br^{87} and Br^{88} have been determined as a function of pressure for plate spacings of 2, 6 and 34 mm. The curve obtained from the 2 mm. spacing is shown in Fig. 17. All three spacings gave a curve which was linear in the range of pressure used; 1 to 3 atmospheres. The linear dependence indicates that all of the measurements have been made in a region where the range of the fission recoils is greater than the geometrical dimensions of the cell.

In the case of the 34 mm. plate spacing, the space between the plates is greater than the range of the recoils. The major portion of the recoils must, however, leave the plate obliquely and strike the side walls rather than the opposite plate. As the side walls are relatively close to the plates, the range of the recoils is still large compared to the available space.

(iv) Contribution of Secondary Bromine

For each of the three nuclides studied, production of organically-bound bromine resulted from hot-atom reaction of a bromine atom activated

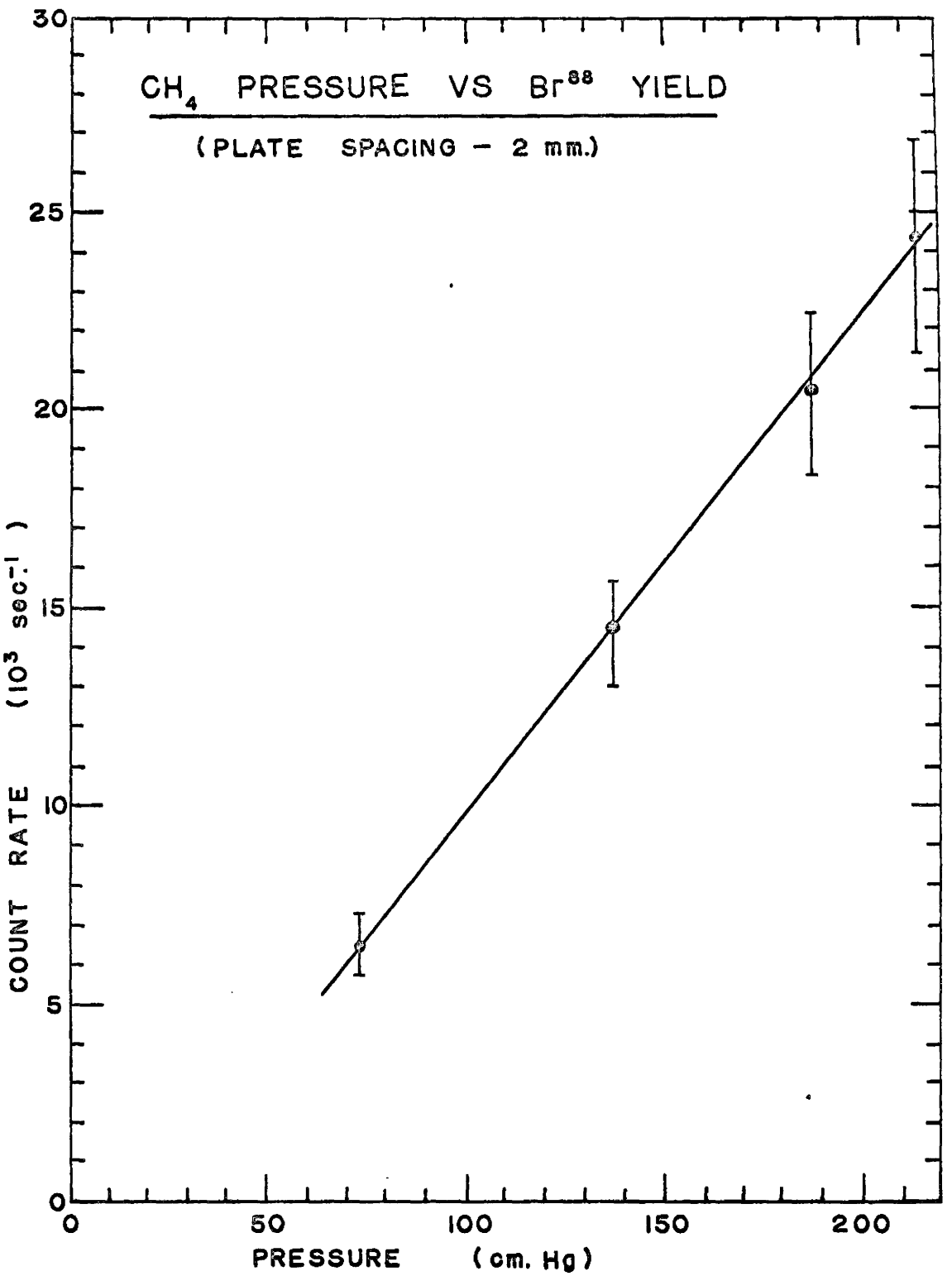
CH4 PRESSURE VS Br88 YIELD
(PLATE SPACING – 2 mm.)
COUNT RATE (10³ sec⁻¹)
PRESSURE (cm. Hg)
0
5
10
15
20
25
30
0
50
100
150
200

Fig. 17

by either of two modes: directly by the fission act itself

$$U^{235}\ (n,F)\ Br^{87},\ Br^{88},\ Br^{89} \qquad \text{(Primary)}$$

or by beta decay of its precursors

$$As^{87,88,89} \xrightarrow{\beta^-} Se^{87,88,89} \xrightarrow{\beta^-} Br^{87,88,89} \quad \text{(Secondary)}$$

The primary process produces bromine only during the neutron irradiation. When the irradiation ends primary bromine production ceases, but the secondary process continues producing bromine from the decay of the arsenic and selenium. The secondary process continues until all of the precursors have decayed to bromine. The method used to distinguish between the two modes of production was based upon a determination of the time during which the activity was produced. Two types of experiments were carried out; these will be labelled "P" type and "S" type experiments.

The "P" type experiment involved irradiation for one half-life of the selenium parent. This was followed by immediate sweeping of the organic material from the cell to the traps. During the irradiation the bromine was produced, mainly by the primary process. Less than one-third of the parent undergoes beta decay to bromine during the irradiation. The remainder decays to bromine subsequent to the irradiation. (The derivation of these values is presented in Appendix II). Attempts were made to collect the bromine activity produced subsequent to the irradiation. These were unsuccessful due to incomplete removal of the bromine activity in the first sweep of the cell.

The "S" type experiment, like the "P" type, involved an irradiation for one half-life of the selenium parent. In the "S" type experiment the sweeping process was delayed for a period, allowing the precursors to undergo beta decay to bromine before sweeping. The bromine activity

produced during the delay time was produced entirely by the beta decay of its precursors.

The half-lives of the precursors of the short-lived bromine isotopes have been determined by Satizahn (82) and Williams (31). Satizahn measured the half-lives of Se^{84} and Se^{86}* and reported values of 3.3 ± 0.2 min. and 17 ± 3 sec. respectively. Williams estimated the half life of Se^{87} to be 5 to 10 seconds.

The "P" and "S" experiments were carried out with Br^{84}, Br^{86} and Br^{87}; no attempt was made with Br^{88} and Br^{89} as their precursors' half-lives would be expected to be too short to be studied with this apparatus. The irradiation and delay times used in the experiments are shown in Table XVII.

The differences between the yields of the "P" and "S" type experiments, when corrected for beta decay during the irradiation, length of delay time, and decay, gave the relative contributions of the secondary bromine. The relative contributions of the two modes of production are shown in Table XVIII. The experiments with Br^{84} show the two methods of production give comparable yields. In Br^{86} an upper limit of 10 ± 10% was set. No significant difference was observed between the "P" and "S" experiments with Br^{87}, thus no secondary yield could be assigned to it; all of the Br^{87} appears to have come from the primary process. It is

---

* Satizahn originally assessed the 17 ± 3 sec. activity to be Se^{87} decaying to a one minute Br^{87}. On the basis of Williams' work it appears that the 17 ± 3 sec. activity is Se^{86} decaying to one min. Br^{86}, which was unknown when Satizahn did his work.

TABLE XVII

Irradiation Procedure for Measurement of Contribution of Secondary Bromine

Isotope	Type of Experiment	Irradiation Time	Delay Time
84	P	3.2 min.	0
	S	3.2 min.	3.2 min.
86	P	15 sec.	0
	S	15 sec.	30 sec.
87	P	5 sec.	0
	S	5 sec.	20 sec.

TABLE XVIII

Relative Contributions of Primary and Secondary Bromine

Isotope	Primary*	Secondary
84	1.0 ± 0.2	1.1 ± 0.2
86	1.0 ± 0.1	0.1 ± 0.1
87	no secondary observed	

*Data normalized to primary; primary = 1.0

likely that Br^{88} and Br^{89} would also be produced exclusively by the primary process.

Both Br^{84} and Br^{86} were detected by gamma spectroscopy. Measurements were made of the 0.879 and 1.56 MeV photopeaks of the Br^{84} and Br^{86}* respectively. Br^{87} was measured by delayed-neutron counting and analysis by MADCAP to give the relative intensity of the 55.8 second component of the decay curve.

(v) Delayed-Neutron Yields

The decay of the delayed-neutron emission from bromine was measured at various plate spacings and irradiation times. This was done in order to show any systematic variations with irradiation time or geometry. Decay curves were obtained by multi-channel scaling at intervals of 2 sec. per channel. The first point was obtained 11 sec. after the end of the irradiation. A typical decay curve is shown in Fig. 18.

The decay curves were analyzed by the computer program MADCAP to obtain the intensities of Br^{87}, Br^{88} and Br^{89}, using the half-lives obtained in section (ii) of this chapter (Table XV). The intensities were divided by $(1 - e^{-\lambda t})$ to obtain the yields for infinite irradiation; these yields were then normalized to Br^{88} for comparison.

U^{235}: The relative yields are shown in Table XIX for various irradiation times. Their results are consistent except at very short irradiation times. The problem here can be explained by difficulties in timing the irradiation and by poor counting statistics due to the low count rates.

---

*Br^{86} was present with a comparable quantity of Br^{87}. Considerable error is expected in any attempt to isolate one peak from this complex spectrum.

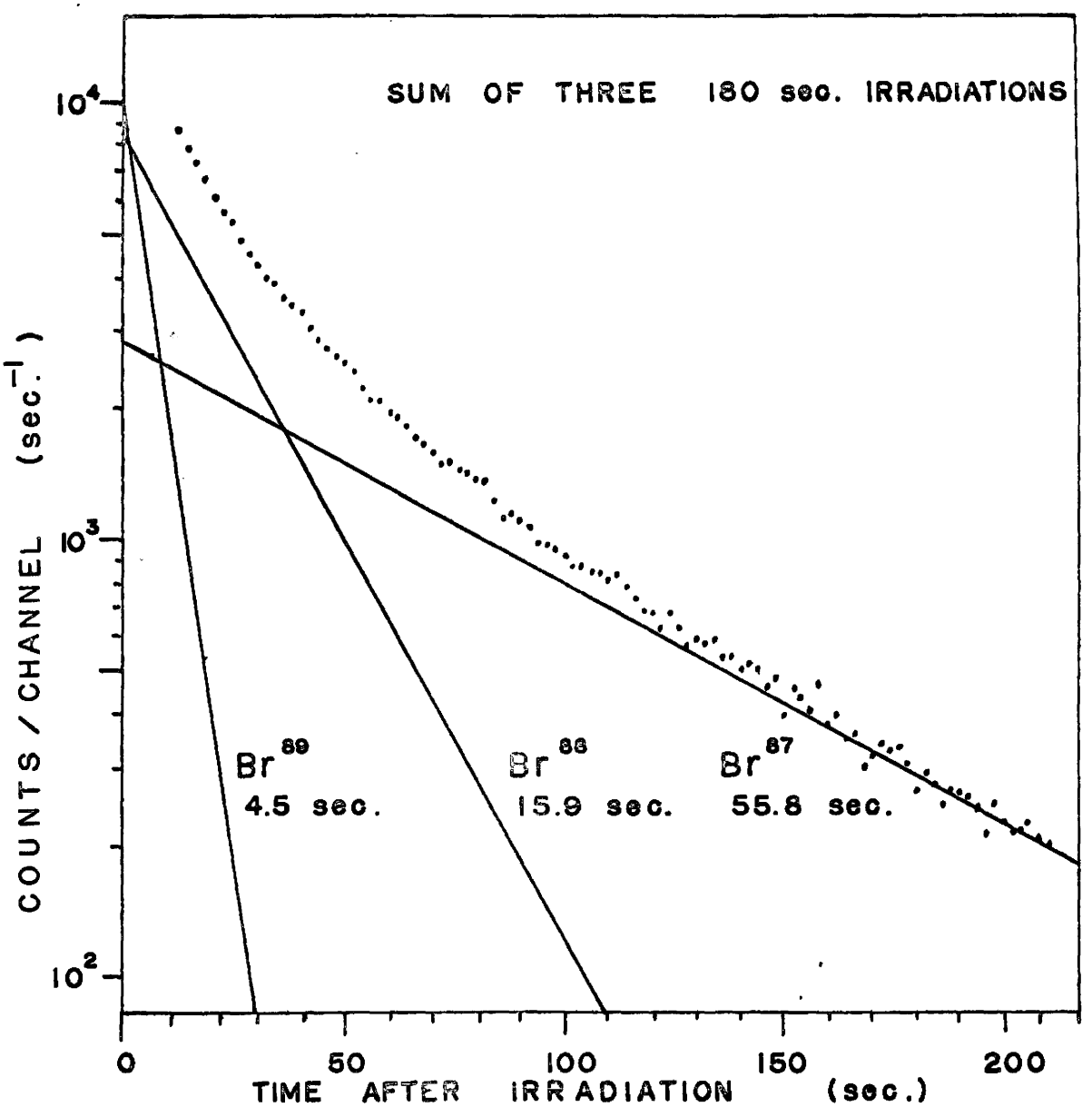

Fig. 18 DECAY OF DELAYED - NEUTRON ACTIVITY FROM BROMINE

Table XX shows the relative yields at various plate spacings; the observed yields are the same at all spacings.

The "best" values for the relative delayed-neutron yields from U^{235} are shown in Table XXII. These were obtained from a large number of decay curves summed together to reduce the statistical spread of the data points.

U^{233}: The relative yields of the delayed-neutron from U^{233} were obtained in the same manner as those for U^{235}. The relative yields for various irradiation times are shown in Table XXI. The "best" values were obtained by summing a large number of decay curves. They are shown in Table XXII along with the U^{235} values.

TABLE XIX

Relative Yields of Delayed Neutrons From Br^{87}, Br^{88} and Br^{89} Produced in Thermal-Neutron Fission of U^{235} Measured at Various Irradiation Times*

Irradiation Time	Y_{87}/Y_{88}	Y_{89}/Y_{88}
6	0.27	1.2
10	0.32	1.3
16	0.34	1.2
60	0.34	1.2
120	0.34	1.4
180	0.35	1.2
480	0.37	1.2
Mean	0.34 ± 0.02	1.2 ± 0.1

* Plate spacing of 6 mm.

TABLE XX

Relative Yields of Delayed Neutrons from Br^{87}, Br^{88} and Br^{89} Produced in Thermal-Neutron Fission of U^{235} Measured at Various Plate Spacings

Plate Spacing	Y_{87}/Y_{88}	Y_{89}/Y_{88}
2 mm.	0.34 ± 0.02	1.0 ± 0.2
6 mm.	0.33 ± 0.02	1.2 ± 0.1
3.4 cm.	0.33 ± 0.02	1.2 ± 0.1

TABLE XXI

Relative Yields of Delayed Neutrons From Br^{87}, Br^{88} and Br^{89} produced in the Thermal-Neutron Fission of U^{233} at Various Irradiation Times

Irradiation Time	Y_{87}/Y_{88}	Y_{89}/Y_{88}
16 sec.	0.55	0.9
60	0.56	0.6
180	0.55	0.7
480	0.54	0.6
Mean	0.55 ± 0.01	0.7 ± 0.2

TABLE XXII

Mean Values* of Relative Yields of Delayed Neutrons From Br^{87}, Br^{88} and Br^{89} Produced in the Thermal-Neutron Fission of U^{233} and U^{235}

Isotope	Y_{87}/Y_{88}	Y_{89}/Y_{88}
233	0.56 ± 0.02	0.6 ± 0.1
235	0.33 ± 0.02	1.2 ± 0.1

* Taken from Composite Decay Curves

CHAPTER V

DISCUSSION

(i) Contribution of Secondary Bromine

The experiments reported in Chapter IV, Section iv have measured the relative yields of organically-bound bromine produced as primary and secondary fission products. These measured yields are shown in Table XXIII along with the predicted yields calculated in Appendix III.

The experiments with Br^{84} show essentially equal yields of organically-bound bromine produced by the primary and secondary processes. The calculated yields would have predicted 35 times more secondary Br^{84} than primary Br^{84}; 35 times that obtained. This indicates that the secondary process enters organic combination with an efficiency only about 3 percent that of the primary process. This value could, however, be a factor of 2 or 3 in error as it is based on a predicted yield, the accuracy of which has not been verified.

A similar result was obtained with the Br^{86} experiments. The measured yield of secondary Br^{86} was one tenth that of the primary Br^{86}. Production of 3.0 times as much of the secondary Br^{86} as the primary would have been predicted; 30 times that obtained. As with the Br^{84}, the Br^{86} also indicates an efficiency of about 3 percent for the secondary process compared to the primary process. Br^{86} being closer to the most probable charge for its mass chain than the Br^{84}, the possibility of error is lower in the prediction but the uncertainty is higher in the measurement. The value could easily be in error by a factor of 2 or 3.

TABLE XXIII

Ratio of Primary to Secondary Yields

Isotope	Measured		Calculated*	
	Primary	Secondary	Primary	Secondary
Br^{84}	1.0 ± 0.2	1.1 ± 0.2	1.0	34.8
Br^{86}	1.0 ± 0.1	0.1 ± 0.1	1.0	3.0
Br^{87}	No secondary detected		1.0	1.1
Br^{88}			1.0	0.45
Br^{89}			1.0	0.15

* Calculated in Appendix III, based on Empirical Zp function and gaussian charge distribution with c = 0.95.

No contribution from secondary Br^{87} was detected in the experiments. Two explanations are possible to explain the lack of secondary Br^{87}. As the predicted yields would indicate approximately equal proportions of primary and secondary Br^{87}, an efficiency of about 3 percent would not produce sufficient secondary Br^{87} to be seen above the experimental error in the measurements.

A less likely explanation would be a very short half-life for the Se^{87} parent. If the half-life of Se^{87} is much shorter than the 5 to 10 seconds estimated by Williams (31), all of the Se^{87} would have decayed to Br^{87} before sweeping from the cell. No secondary Br^{87} would have been observed in this experiment if this were true.

On the basis of the Br^{84} and Br^{86} experiments, the hot-atom process appears to be about 3 percent as efficient with secondary bromine as it is with primary bromine. No secondary Br^{87} was seen; it seems reasonable to assume that its yield was below the experimental error in measurement. The shorter-lived bromine isotopes contain much lower proportions of secondary bromine than do the longer-lived bromine isotopes. It would thus be expected that the contributions from secondary Br^{88} and Br^{89} are even smaller than that of the secondary Br^{87}. If the value of 3 percent were in error a factor of two or three it would likely have no serious effect on the organic yields of the short-lived isotopes.

The experiments have shown that the hot-atom yield of secondary bromine is much lower than that of primary bromine. Several arguments have been put forth, but none seem to fully explain the large differentiation between the two processes.

Denschlag et al (66,67) suggested that the contribution of secondary iodine reacting with methane was also low. Although they did not directly measure the secondary iodine, they attributed a contribution of about 5 percent to the secondary process in order to account for their data.

They assumed the low yield of secondary halogen to be due to the low recoil energies available from the beta decay of the precursors. Although exact values of the beta-recoil energies require a knowledge of the decay schemes of the precursors, it would be expected that beta-decay energies are high. Appendix I shows the recoil energies available from beta decay; it can be seen that many hundreds of electron volts of recoil energy are available at the higher beta-decay energies. Although all of the beta-decay products will not have these high recoil energies, those that do would be expected to undergo hot-atom reactions similar to those of the fission recoils. Those that have insufficient recoil energy will not react, thereby reducing the relative efficiency of the secondary process compared to the primary process. It is unlikely, however, that the large differentiation (a factor of 30) between the processes can be accounted for solely upon the lower recoil energy from beta decay compared to the fission process.

The experiments in this work indicate that the low yield of secondary bromine is due in part to the loss of the precursors to the walls. The loss to the walls can be divided into two groups; those that are lost by impact of fission recoils with the walls and those that are lost by diffusion to the walls.

The dimensions of the cell are small compared to the range of the fission fragments. Many of them will strike the walls with sufficient kinetic energy to be imbedded deeply inside. Once trapped inside the

walls, there is little likelihood that they will be ejected by subsequent beta decay, nor are they likely to get out by diffusion processes. This process should cause no differentiation between primary and secondary bromine as bromine and its precursors are lost to the walls in comparable quantities.

Selenium (or tellurium) stopped in the gas, however, is likely to diffuse to the walls prior to beta decay. Once on the wall, recoil from beta decay will eject comparable quantities into the gas and into the walls. This could reduce the yield for the secondary process by a factor of about two relative to the primary process. A rougher surface could increase the factor somewhat, but not likely by a factor as high as the observed factor of about thirty.

(ii) Relative Yields of the Delayed-Neutron Precursors in Fission

The delayed-neutron yields obtained in Chapter IV section v are shown in Table XXIV corrected, assuming a 3 percent contribution from secondary bromine. The yields now represent the delayed neutrons from primary bromine alone. The yields from U^{235} differ from those of Perlow and Stehney (22) shown in Table IV. This is expected as their values included secondary bromine as well as primary.

Knowing the probabilities of delayed-neutron emission from Br^{87}, Br^{88} and Br^{89} (See Table VI), it was possible to obtain the relative yields of the three delayed-neutron precursors in fission. The assumption was made that all three bromine isotopes entered organic combination with equal efficiency; this assumption appeared to be valid as the three isotopes are formed with approximately the same recoil energy. The relative yields of the three delayed-neutron precursors in fission were obtained

TABLE XXIV

Relative Yields of Delayed Neutrons From Primary Br^{87}, Br^{88} and Br^{89} Produced in the Thermal-Neutron Fission of U^{233} and U^{235}*

Fissioning Nuclide	Br^{87}	Br^{88}	Br^{89}
U^{233}	0.55 ± 0.02	1.0 ± 0.1	0.6 ± 0.1
U^{235}	0.32 ± 0.02	1.0 ± 0.1	1.2 ± 0.1

* Corrected for Contribution from Secondary Bromine.

by correction of the delayed-neutron yields by their respective efficiencies for delayed-neutron emission. As the delayed neutrons have been attributed solely to primary-produced bromine, the yields obtained represent the relative primary yields of Br^{87}, Br^{88} and Br^{89} in fission.

Unfortunately, no primary yields have been measured for the production of Br^{87}, Br^{88} and Br^{89} in fission; thus no comparison can be made with measured values. It is possible, however, to predict what the yields should be and to compare these calculated yields with the measured values.

In Appendix III yields have been calculated and tabulated, based upon a gaussian charge distribution of the form postulated by Glendenin (83)

$$P(Z) = \frac{1}{(c\pi)^{\frac{1}{2}}} \; e^{-(Z-Z_p)^2/c}$$

The values of Zp, the most probable charge in fission, were obtained on the basis of equal charge displacement, ECD, using Z_A values derived from mass formulae of Swiatecki (84) and Seeger (85), and from empirical values derived by Wahl et al (86). The values of c which were used were 1.5, the value postulated by Glendenin (83) and 0.95, the more recent value of Wahl et al (86).

Tables XXV and XXVI show the relative yields obtained from the delayed-neutron measurements (the predicted yields are shown in paranthesis for comparison). The measured yields have been obtained by normalization of the relative fission yields to the predicted yields at Br^{88}.

The measured fission yields contain a large uncertainty, about 25 percent. This uncertainty comes from two sources: the fitting of the intensities to the decay curves and the correction for delayed-neutron emission possibilities.

TABLE XXV

Measured Yields of Br^{87}, Br^{88}, and Br^{89} Produced as Primary Fission Products in the Thermal-Neutron Fission of U^{233}*

Calculation**	Br^{87}	Br^{88}	Br^{89}
	C = 0.95		
ECD - Swiatecki	3.0 ± 0.8 (2.6)	2.9 ± 0.7 (2.9)	1.5 ± 0.4 (1.8)
ECD - Seeger	3.0 ± 0.8 (2.6)	2.9 ± 0.7 (2.9)	1.5 ± 0.4 (1.8)
	C = 1.5		
ECD - Swiatecki	2.5 ± 0.6 (2.1)	2.4 ± 0.6 (2.4)	1.2 ± 0.3 (1.8)
ECD - Seeger	2.5 ± 0.6 (2.1)	2.4 ± 0.6 (2.4)	1.2 ± 0.3 (1.8)

* Yields normalized to calculated yields of Br^{88}. Predicted yields are in parentheses. Yields are in percent.

** Zp values calculated by Fiedler (87) on basis of ECD using Z_A values derived from mass formulae of Swiatecki (84) and Seeger (85).

TABLE XXVI

Measured Yields of Br^{87}, Br^{88} and Br^{89} Produced as Primary Fission Products in the Thermal Neutron Fission of U^{235}*

Calculation	Br^{87}	Br^{88}	Br^{89}
	C = 0.95		
Empirical - Wahl	1.3 ± 0.3 (1.1)	2.1 ± 0.5 (2.1)	2.2 ± 0.5 (2.3)
ECD-Swiatecki	1.2 ± 0.3 (1.0)	2.0 ± 0.5 (2.0)	2.1 ± 0.5 (2.1)
ECD - Seeger	1.3 ± 0.3 (1.1)	2.1 ± 0.5 (2.1)	2.2 ± 0.5 (2.2)
	C = 1.5		
Empirical - Wahl	1.0 ± 0.4 (1.0)	1.6 ± 0.4 (1.6)	1.7 ± 0.4 (2.0)
ECD - Swiatecki	1.0 ± 0.4 (1.0)	1.6 ± 0.4 (1.6)	1.7 ± 0.4 (2.0)
ECD - Seeger	1.0 ± 0.4 (1.0)	1.6 ± 0.4 (1.6)	1.7 ± 0.4 (2.0)

* Yields normalized to calculated yield of Br^{88}. Predicted yields are in paremtheses. Yields are in percent.

** Zp values are empirical by Wahl (86) and calculated on basis of ECD using Z_A values derived from mass formulae of Swiatecki (84) and Seeger (85).

The uncertainties in fitting the intensities to the decay data were obtained by the computer program MADCAP. The intensities were fitted to the decay data with an uncertainty usually less than ten percent, but the intensities obtained usually had a spread of 20 percent about a mean value.

The spread in the intensity values could be reduced by summation of a series of decay curves and analysis of the composite. The composite decay curve had a much lower spread in its data points allowing the computer to fit the data with much greater certainty. The spread in the computed values was also much lower. An upper limit of ten percent was given to the uncertainty in the relative yields obtained.

Determination of the fission yields from the neutron yields greatly increased the relative errors. This occurred due to the large uncertainty in the neutron-emission probabilities measured by Aron (39); these had an uncertainty of 20 percent. The uncertainty in these values plus those in the measured neutron yields gave values for the relative fission yields which had an uncertainty of about 25 percent.

The measured yields are in excellent agreement with the predicted yields. The size of the uncertainty prevents much preference of one set of predicted yields over another. The U^{233} results do, however, show a preference to Wahl's (86) value of c of 0.95, in preference to the Glendenin (83) value of 1.5. The Glendenin value predicted a yield of Br^{89} which is high compared to the measured value; the use of the lower value of c gave better agreement with the data.

The agreement of the data with the postulate of equal charge displacement gives further evidence to the postulate's useful character. It is however only an empirical relationship having no theoretical basis.

With the further support that this data gives to the postulate of equal charge displacement, it is hoped that some theory may be developed which will explain why it is so successful.

BIBLIOGRAPHY

(1) O. Hahn and F. Strassman, Naturwiss. 27 11 (1939).

(2) L. Szilard and W. H. Zinn, Phys. Rev. 55 779 (1939).

(3) N. Bohr and J. A. Wheeler, Phys. Rev. 56 426 (1939).

(4) J. Frankel, J. Phys. USSR 1 125 (1939).

(5) R. Roberts, R. Meyer and P. Wang, Phys. Rev. 55 510 (1939)
R. Roberts, R. Meyer, L. Hafstad, and P. Wang, Phys. Rev. 55 510 (1939).

(6) G. R. Keepin, "Progress in Nuclear Energy", Vol. 1,
Permagon Press, London (1956).

(7) G. R. Keepin, J. Nuclear Energy 6 1 (1957).

(8) G. R. Keepin, Nucleonics 20 No.8 150 (1962).

(9) E. K. Hyde, UCRL - 9036 - Rev. (1962).

(10) G. R. Keepin, T. F. Wimett and R. K. Zeigler, Phys. Rev. 107 1044 (1957).

(11) D. J. Hughes, J. Dabbs, A. Cahn, and D.B. Hall, Phys. Rev. 74 1330 (1948).

(12) M. Burgy, L. A. Pardue, A. B. Willard and E. O. Wollan, Phys. Rev.
70 104 (1946).

(13) T. W. Bonner, S. J. Bame Jr. and J. E. Evans. Phys. Rev. 101 1514 (1956).

(14) E. Fermi, Declassified Document CP-1088 (1943).

(15) R. Batchelor and H. R. McK. Hyder, J. Nuclear Energy 3 7 (1956).

(16) R. Batchelor, R. Aves and T.H.R. Skyrme, Rev. Sci. Inst. 26 1037 (1955).

(17) O. Hahn and F. Strassman, Naturwiss. 28 817 (1940).

(18) H. J. Born and W. Seelman - Eggeberg, Naturwiss. 31 59 (1943);
31 86 (1943).

(19) V. Reizler, Naturwiss. 31 326 (1943).

(20) A. H. Snell, J. S. Levinger, E. P. Meiners, M. B. Sampson and
R. G. Wilkinson, Phys. Rev. 72 545 (1947).

(21) G. J. Perlow and A. F. Stehney, Phys. Rev. 107 776 (1957).

(22) G. J. Perlow and A.F. Stehney, Phys. Rev. 113 1269 (1959).

(23) A. L. Gardner, N. Knable and B. J. Boyer, Phys. Rev. 83 1054 (1951).

(24) L. W. Alvarez, Phys. Rev. 75 1127 (1949).

(25) G. J. Perlow, W. J. Ramler, A. F. Stehney and J. L. Yutema, Phys. Rev. 122 899 (1961).

(26) J. Gilat, G. D. O'Kelley and E. Eichler, ORNL - 3488.

(27) A. V. Kogan, Soviet Physics Doklady 1 372 (1947).
A. V. Kogan and L. I. Rusinov, Soviet Physics JETP 5 365 (1957).

(28) E. Feenberg and G. Trigg, Rev. Mod. Phys. 22 399 (1950).

(29) S. A. Moszkowski, Phys. Rev. 82, 35 (1951).

(30) A. F. Stehney and N. Sugarman, Phys. Rev. 89 194 (1953).

(31) E. T. Williams, Ph.D. Thesis, Massachusetts Institute of Technology, Cambridge (1963).

(32) C. D. Coryell, Ann. Rev. Nucl. Sci. 2 305 (1953).

(33) K. Way and M. Wood, Phys. Rev. 94 119 (1954).

(34) A. C. Pappas, M.I.T. Lab. for Nuclear Science Report No. 63 (1953); USAEC Report No. AECU-2086 (unpublished).

(35) J. A. Harvey, Phys. Rev. 81 353(1951).

(36) H. B. Levey, Phys. Rev. 106 1265 (1957).

(37) J. M. Blatt and V. F. Weisskopf, "Theoretical Nuclear Physics", John Wiley and Sons, N. Y. (1952).

(38) H. Feshbach, C. E. Porter and V. F. Weisskopf, Phys. Rev. 96 448 (1954).

(39) I. M. Aron, O. I. Kostochkin, K. A. Petrzhak, and U. I. Shpakov, Atomnaya Energiya 16 368 (1964).

(40) G. R. Keepin, J. Nuclear Energy 7 13 (1958).

(41) S. Katkoff, Nucleonics 8 No. 11 201 (1960).

(42) W. E. Nervik, Phys. Rev. 119 1685 (1960).

(43) P. Fong, Phys. Rev. 102 434 (1956).

(44) A. Bohr, Paper No. P/911 in the "Proceedings of the International Conference on the Peaceful Uses of Atomic Energy", vol. 2, United Nations, New York (1956).

(45) I. T. Kristyuk, Atomnaya Energiya 16 146 (1964).

(46) R. L. Murray "Introduction to Nuclear Engineering", Prentice Hall, New York (1955).

(47) J. E. Willard, Ann. Rev. Nucl. Sci. 3 193 (1953).

(48) J. E. Willard, Ann. Rev. Phys. Chem. 6 141 (1955).

(49) J. E. Willard, Nucleonics 19 No. 10 61 (1961).

(50) G. Harbottle and N. Sutin, "Advances in Inorganic Chemistry and Radiochemistry ", Academic Press Inc., New York (1959).

(51) A. P. Wolf, Ann. Rev. Nucl. Sci. 10 259 (1960).

(52) P. J. Estrup and R. Wolfgang, J. Am. Chem. Soc. 82 2665 (1960).

(53) J. F. Hornig, G. Levey and J. E. Willard, J. Chem. Phys. 20 1556 (1952).

(54) S. Wexler and G. R. Anderson, J. Am. Chem. Soc. 76 4678 (1954).

(55) J.C.D. Milton and J. S. Fraser , Can. J. Phys. 40 1626 (1962).

(56) F. Schroth and J. P. Adloff, J. Chim. Physique 61 1373 (1964).

(57) J. C. W. Chien and J. E. Willard, J. Am. Chem. Soc. 75 6160 (1953).

(58) A. A. Gordus and J. E. Willard, J. Am. Chem. Soc. 79 4609 (1957).

(59) E. P. Rack and A. A. Gordus, J. Chem. Phys. 34 1855 (1961); J. Phys. Chem. 65 945 (1961).

(60) L. Friedman and W. F. Libby, J. Chem. Phys. 17 647 (1949).

(61) M. S. Fox and W. F. Libby, J. Chem. Phys. 20 487 (1952).

(62) J. B. Evans and W. E. Willard, J. Am. Chem. Soc. 78 2908 (1956).

(63) J. B. Evans, Ph.D. Thesis, University of Wisconsin, Madison (1957).

(64) M. D. Silbert and R. H. Tomlinson, Can. J. Chem. 39 706 (1961).

(65) F. S. Rowland and R. L. Wolfgang, Rev. Sci. Inst. 29 210 (1958).

(66) H. O. Denschlag, N. Henzel and G. Herrman, Paper presented at the "Discussions on Nuclear Chemistry", Oxford (1962).

(67) H. O. Denschlag, N. Henzel and G. Herrman, Radiochemica Acta 1 172 (1963).

(68) D. W. Ockenden and R. H. Tomlinson, Can. J. Chem. 40 1594 (1962).

(69) G. Herrman, Private Communication (1963).

(70) J. K. Bøggild, L. Minnhagen and O. B. Nielson, Phys. Rev. 76 988 (1949).

(71) J. K. Bøggild, O. H. Arrøe and T. Sigurgeirsson, Phys. Rev. 71 281

(72) J. W. Hallam, Ms.Sc. Thesis, McMaster University (1961).

(73) M. D. Silbert and R. H. Tomlinson, Nucleonics 20 No. 2 73 (1962).

(74) D. J. Hughes and J. A. Harvey, BNL - 325 (1955).

(75) N. P. Archer, Unpublished Data (1964).

(76) Handbook of Chemistry and Physics (44th Ed.), Chemical Publishing Co., Cleveland, Ohio (1963).

(77) N. Brenner, E. Cieplinski, L. S. Ettre and V. J. Coates, J. Chromat. 3 230 (1960).

(78) W. E. Harris and W. H. McFadden, Anal. Chem. 31 114 (1959).

(79) Nuclear Data Sheets, Nat. Acad. Sci., N.R.C., (U.S. Gov't. Printing Office, Washington, D.C.).

(80) N. Sugarman, J. Chem. Phys. 17 11 (1949).

(81) N. R. Johnson and G. D. O'Kelley, Phys. Rev. 108 82 (1957).

(82) J. E. Satizahn, J. D. Knight and M. Kahn, J. Inorg. and Nucl. Chem. 12 206 (1960).

(83) L. E. Glendenin, C. D. Coryell and R. R. Edwards, "Radiochemical Studies: The Fission Products" , C. D. Coryell and N. Sugarman, editors, National Nuclear Energy Series, Plutonium Project Record, McGraw-Hill Book Co. Inc., New York (1951).

(84) W. J. Swiatecki, private communication to J. Fiedler (1965).

(85) P. A. Seeger, Nuclear Physics 25 1 (1961).

(86) A. C. Wahl, R. L. Ferguson, D. R. Nethaway, D. E. Troutner and K. Wolfsberg, Phys. Rev. 126 112 (1962).

(87) J. Fiedler, Unpublished Data (1965).

APPENDIX I

CALCULATION OF RECOIL ENERGIES GIVEN TO NUCLEI BY RADIOACTIVE DECAY

The kinetic energy given to an atom as a result of radioactive decay can be evaulated by equations (1), (2) and (3) below. These expressions have been derived by Wahl and Bonner (88). The recoil energies given to nuclei of masses 87 and 137 have been computed and are shown in Tables XXVII and XXVIII respectively.

Alpha Decay: The recoil energy from alpha decay is given by

$$E_M = \frac{m}{M} E_\alpha \qquad (1)$$

where E_M and E_α are the kinetic energies of the recoiling atom and the alpha particle respectively. M and m are the respective masses of the recoil atom and the alpha particle. E_M and E_α are in the same energy units.

Beta Decay: A rigorous treatment of beta-decay recoil energies was not used; no corrections for neutrino emission were included. The recoil energy from beta decay is given by

$$E_M = 541 \frac{E_e}{M} + 536 \frac{E_e^2}{M} \text{ eV} \qquad (2)$$

which gives the maximum recoil energy that can be obtained from a beta decay. The average recoil energy will be somewhat lower. If the energy of the electron, E_e is given in MeV and the mass of the recoil atom, M, is given in atomic mass units, the recoil energy E_M, will be in eV.

Gamma Emission: The recoil energy available from gamma emission is given by

$$E_M = 536 \frac{E_\gamma^2}{M} \text{ eV} \qquad (3)$$

where E_γ and M are in MeV and atomic mass units respectively giving the recoil energy E_M in eV. The expression will be somewhat more complicated if a number of gamma rays are given off. The expression will then include terms for each gamma ray and their angular dependences.

(88) A.C. Wahl and N.A. Bonner, "Radioactivity Applied to Chemistry", John Wiley and Sons, Inc., New York (1951).

TABLE XXVII

RECOIL ENERGIES FROM RADIOACTIVE DECAY

MASS=87

ENERGY	ALPHA	BETA	GAMMA
0.1 MEV	0.0046 MEV	0.68 EV	0.06 EV
0.2	0.0092	1.49	0.25
0.3	0.0138	2.42	0.55
0.4	0.0184	3.47	0.99
0.5	0.0230	4.65	1.54
0.6	0.0276	5.95	2.22
0.7	0.0322	7.37	3.02
0.8	0.0368	8.92	3.94
0.9	0.0414	10.59	4.99
1.0	0.0460	12.38	6.16
1.1	0.0506	14.29	7.45
1.2	0.0552	16.33	8.87
1.3	0.0598	18.50	10.41
1.4	0.0644	20.78	12.08
1.5	0.0690	23.19	13.86
1.6	0.0736	25.72	15.77
1.7	0.0782	28.38	17.81
1.8	0.0828	31.15	19.96
1.9	0.0874	34.06	22.24
2.0	0.0920	37.08	24.64
2.1	0.0966	40.23	27.17
2.2	0.1013	43.50	29.82
2.3	0.1059	46.89	32.59
2.4	0.1105	50.41	35.49
2.5	0.1151	54.05	38.51
2.6	0.1197	57.82	41.65
2.7	0.1243	61.70	44.91
2.8	0.1289	65.71	48.30
2.9	0.1335	69.85	51.81
3.0	0.1381	74.10	55.45
3.1	0.1427	78.48	59.21
3.2	0.1473	82.99	63.09
3.3	0.1519	87.61	67.09
3.4	0.1565	92.36	71.22
3.5	0.1611	97.24	75.47
3.6	0.1657	102.23	79.85
3.7	0.1703	107.35	84.34
3.8	0.1749	112.59	88.96
3.9	0.1795	117.96	93.71
4.0	0.1841	123.45	98.57

TABLE XXVII (CONTD.)

RECOIL ENERGIES FROM RADIOACTIVE DECAY

MASS=87

ENERGY	ALPHA	BETA	GAMMA
4.1 MEV	0.1887 MEV	129.06 EV	103.57 EV
4.2	0.1933	134.80	108.68
4.3	0.1979	140.65	113.92
4.4	0.2025	146.64	119.28
4.5	0.2071	152.74	124.76
4.6	0.2117	158.97	130.37
4.7	0.2163	165.32	136.09
4.8	0.2209	171.80	141.95
4.9	0.2255	178.39	147.92
5.0	0.2301	185.11	154.02
5.1	0.2347	191.96	160.25
5.2	0.2393	198.93	166.59
5.3	0.2439	206.02	173.06
5.4	0.2485	213.23	179.65
5.5	0.2531	220.57	186.37
5.6	0.2577	228.03	193.21
5.7	0.2623	235.61	200.17
5.8	0.2669	243.32	207.25
5.9	0.2715	251.15	214.46
6.0	0.2761	259.10	221.79
6.1	0.2807	267.18	229.25
6.2	0.2853	275.38	236.83
6.3	0.2899	283.70	244.53
6.4	0.2945	292.15	252.35
6.5	0.2991	300.72	260.30
6.6	0.3038	309.41	268.37
6.7	0.3084	318.23	276.56
6.8	0.3130	327.17	284.88
6.9	0.3176	336.23	293.32
7.0	0.3222	345.41	301.89
7.1	0.3268	354.72	310.57
7.2	0.3314	364.15	319.38
7.3	0.3360	373.71	328.32
7.4	0.3406	383.39	337.37
7.5	0.3452	393.19	346.55
7.6	0.3498	403.11	355.85
7.7	0.3544	413.16	365.28
7.8	0.3590	423.33	374.83
7.9	0.3636	433.63	384.50
8.0	0.3682	444.05	394.30

TABLE XXVII (CONTD.)

RECOIL ENERGIES FROM RADIOACTIVE DECAY

MASS=87

ENERGY	ALPHA	BETA	GAMMA
8.1 MEV	0.3728 MEV	454.59 EV	404.22 EV
8.2	0.3774	465.25	414.26
8.3	0.3820	476.04	424.43
8.4	0.3866	486.95	434.71
8.5	0.3912	497.98	445.13
8.6	0.3958	509.14	455.66
8.7	0.4004	520.42	466.32
8.8	0.4050	531.82	477.10
8.9	0.4096	543.35	488.01
9.0	0.4142	555.00	499.03
9.1	0.4188	566.77	510.19
9.2	0.4234	578.67	521.46
9.3	0.4280	590.69	532.86
9.4	0.4326	602.83	544.38
9.5	0.4372	615.10	556.02
9.6	0.4418	627.49	567.79
9.7	0.4464	640.00	579.68
9.8	0.4510	652.63	591.69
9.9	0.4556	665.39	603.83
10.0	0.4602	678.28	616.09

TABLE XXVIII

RECOIL ENERGIES FROM RADIOACTIVE DECAY

MASS=137

ENERGY	ALPHA	BETA	GAMMA
0.1 MEV	0.0029 MEV	0.43 EV	0.04 EV
0.2	0.0058	0.95	0.16
0.3	0.0088	1.54	0.35
0.4	0.0117	2.21	0.63
0.5	0.0146	2.95	0.98
0.6	0.0175	3.78	1.41
0.7	0.0205	4.68	1.92
0.8	0.0234	5.66	2.50
0.9	0.0263	6.72	3.17
1.0	0.0292	7.86	3.91
1.1	0.0321	9.08	4.73
1.2	0.0351	10.37	5.63
1.3	0.0380	11.75	6.61
1.4	0.0409	13.20	7.67
1.5	0.0438	14.73	8.80
1.6	0.0468	16.33	10.02
1.7	0.0497	18.02	11.31
1.8	0.0526	19.78	12.68
1.9	0.0555	21.63	14.12
2.0	0.0585	23.55	15.65
2.1	0.0614	25.55	17.25
2.2	0.0643	27.62	18.94
2.3	0.0672	29.78	20.70
2.4	0.0701	32.01	22.54
2.5	0.0731	34.32	24.45
2.6	0.0760	36.72	26.45
2.7	0.0789	39.18	28.52
2.8	0.0818	41.73	30.67
2.9	0.0848	44.36	32.90
3.0	0.0877	47.06	35.21
3.1	0.0906	49.84	37.60
3.2	0.0935	52.70	40.06
3.3	0.0964	55.64	42.61
3.4	0.0994	58.65	45.23
3.5	0.1023	61.75	47.93
3.6	0.1052	64.92	50.70
3.7	0.1081	68.17	53.56
3.8	0.1111	71.50	56.50
3.9	0.1140	74.91	59.51
4.0	0.1169	78.39	62.60

TABLE XXVIII (CONTD.)

RECOIL ENERGIES FROM RADIOACTIVE DECAY

MASS=137

ENERGY	ALPHA	BETA	GAMMA
4.1 MEV	0.1198 MEV	81.96 EV	65.77 EV
4.2	0.1228	85.60	69.01
4.3	0.1257	89.32	72.34
4.4	0.1286	93.12	75.74
4.5	0.1315	97.00	79.23
4.6	0.1344	100.95	82.79
4.7	0.1374	104.98	86.43
4.8	0.1403	109.10	90.14
4.9	0.1432	113.29	93.94
5.0	0.1461	117.55	97.81
5.1	0.1491	121.90	101.76
5.2	0.1520	126.33	105.79
5.3	0.1549	130.83	109.90
5.4	0.1578	135.41	114.09
5.5	0.1607	140.07	118.35
5.6	0.1637	144.81	122.69
5.7	0.1666	149.62	127.11
5.8	0.1695	154.52	131.61
5.9	0.1724	159.49	136.19
6.0	0.1754	164.54	140.85
6.1	0.1783	169.67	145.58
6.2	0.1812	174.88	150.39
6.3	0.1841	180.16	155.28
6.4	0.1870	185.53	160.25
6.5	0.1900	190.97	165.30
6.6	0.1929	196.49	170.42
6.7	0.1958	202.09	175.63
6.8	0.1987	207.76	180.91
6.9	0.2017	213.52	186.27
7.0	0.2046	219.35	191.71
7.1	0.2075	225.26	197.22
7.2	0.2104	231.25	202.82
7.3	0.2134	237.32	208.49
7.4	0.2163	243.47	214.24
7.5	0.2192	249.69	220.07
7.6	0.2221	255.99	225.98
7.7	0.2250	262.37	231.97
7.8	0.2280	268.83	238.03
7.9	0.2309	275.37	244.17
8.0	0.2338	281.99	250.39

TABLE XXVIII (CONTD.)

RECOIL ENERGIES FROM RADIOACTIVE DECAY

MASS=137

ENERGY	ALPHA	BETA	GAMMA
8.1 MEV	0.2367 MEV	288.68 EV	256.69 EV
8.2	0.2397	295.45	263.07
8.3	0.2426	302.30	269.53
8.4	0.2455	309.23	276.06
8.5	0.2484	316.24	282.67
8.6	0.2513	323.32	289.36
8.7	0.2543	330.49	296.13
8.8	0.2572	337.73	302.98
8.9	0.2601	345.05	309.90
9.0	0.2630	352.45	316.91
9.1	0.2660	359.92	323.99
9.2	0.2689	367.48	331.15
9.3	0.2718	375.11	338.38
9.4	0.2747	382.82	345.70
9.5	0.2776	390.61	353.09
9.6	0.2806	398.48	360.57
9.7	0.2835	406.42	368.12
9.8	0.2864	414.45	375.75
9.9	0.2893	422.55	383.46
10.0	0.2923	430.73	391.24

APPENDIX II

PRODUCTION OF A RADIOACTIVE DAUGHTER BY BETA DECAY OF ITS PARENT DURING AND AFTER IRRADIATION

The production of a daughter by beta decay of its parent can be divided into two parts: production during the irradiation and production after the irradiation. During the irradiation, production of the parent and decay of the parent to its daughter are competitive processes. At short irradiation times, production of the parent is the predominant process with little decay to the daughter. At long irradiation times, the two processes are equally important, the parent decaying as rapidly as it is formed; this sets an upper limit to the attainable parent activity. At the end of the irradiation production of the parent ceases. All parent activity decays to its daughter.

The following treatment presents a derivation of the rate laws for production of a radioactive daughter during and after irradiation of its parent. The irradiation time and post-irradiation times will be represented by t_1 and t_2 respectively.

a. During the Irradiation: The amount of the daughter, N_2, present at the end of the irradiation is calculated from the amount of the parent, N_1, which has decayed during the irradiation. The buildup of the parent is equal to its production rate, P_1, minus its decay rate.

$$\frac{dN_1}{dt_1} = P_1 - N_1\lambda_1 \tag{1}$$

$$N_1 = \frac{P_1}{\lambda_1}\ (1 - e^{-\lambda_1 t_1}) \tag{2}$$

The rate of production of the daughter is equal to the rate of decay of the parent minus its own decay rate.

$$\frac{dN_2}{dt} = N_1\lambda_1 - N_2\lambda_2$$

$$= P_1\ (1 - e^{-\lambda_1 t_1}) - N_2\lambda_2 \tag{3}$$

which can be solved to give

$$N_2 = P_1\ \frac{e^{2\lambda_2 t_1} - e^{\lambda_2 t_1}}{\lambda_2} + \frac{e^{-\lambda_2 t_1}}{\lambda_2 - \lambda_1}\ (1 - e^{(\lambda_2 - \lambda_1)t_1}) \tag{4}$$

If the irradiation time, t_1, is equal to one half-life of the parent, N_2 reduces to

$$N_2 = P_1\ \frac{e^{2\lambda_2 t_1} - e^{\lambda_2 t_1}}{\lambda_2} + \frac{e^{-\lambda_2 t_1}}{\lambda_2 - \lambda_1}\ (1 - \tfrac{1}{2}\, e^{-\lambda_2 t_1}) \tag{5}$$

b. After the Irradiation: After the irradiation, the buildup of the daughter is equal to its production from decay of the parent minus its loss by its own decay.

$$\frac{dN_2}{dt} = N_1\lambda_1 - N_2\lambda_2 \tag{6}$$

At the end of the irradiation the amount of parent produced was given by (2)

$$N_1 = \frac{P_1}{\lambda_1}\ (1 - e^{-\lambda_1 t_1}) \tag{7}$$

The rate of production of the daughter (6) becomes

$$\frac{dN_2}{dt} = \frac{P_1}{\lambda_1} (1 - e^{-\lambda_1 t_1}) e^{-\lambda_1 t_2} - N_2\lambda_2 \qquad (8)$$

which can be solved to give

$$N_2 = \frac{P_1 (1 - e^{-\lambda_1 t_1}) (e^{-\lambda_1 t_2} - e^{-\lambda_2 t_2})}{\lambda_1 (\lambda_2 - \lambda_1)} \qquad (9)$$

which for a waiting period of one half-life reduces to

$$N_2 = \frac{P_1 (1 - e^{-\lambda_1 t_1}) (1/2 - e^{-\lambda_2 t_2})}{\lambda_1 (\lambda_2 - \lambda_1)} \qquad (10)$$

If the irradiation is also one half-life (10) reduces to

$$N_2 = \frac{P_1 (1/2 - e^{-\lambda_2 t_1})}{2\lambda_1 (\lambda_2 - \lambda_1)} \qquad (11)$$

Evaluation of equations (5) and (11) for the Br^{84} experiment carried out in Chapter IV, section iv, shows that an irradiation for one half-life of the precursor, Se^{84}, produces 28% of the Br^{84} during the irradiation and 72% subsequent to the irradiation.

APPENDIX III

CALCULATION OF THE YIELDS OF THE SHORT-LIVED BROMINE ISOTOPES IN FISSION

Glendenin et al (83) postulated, on the basis of experimental measurements, an empirical expression relating the relative yields of the nuclides in a given mass chain produced in fission. The expression is a gaussian-type charge distribution of the following form:

$$P(Z) = \frac{1}{(c\pi)^{\frac{1}{2}}} \; e^{-(Z-Zp)^2/c}$$

P(Z) represents the relative chain yield of a nuclide of charge Z. The expression is normalized such that the sum of all values of P(Z) lying one charge unit apart add to unity.

Two values of the constant, c, have been used in the calculations of fission yields in this section: the original value of about 1.5 proposed by Glendenin et al (83) and a more recent value of about 0.95 proposed by Wahl et al (86). The latter value gives a sharper distribution curve than does the former; it is also in better agreement with the more recent experimental measurements.

The values of Z_p the most probable charge of the fission fragments, used in this work were the empirical values of Wahl et al (86) and the calculated values of Fiedler (87). These are shown for masses 84 to 89 in thermal-neutron fission of U^{233} and U^{235} in tables XXIX and XXX respectively, along with some measured values of Wahl et al (86) and Wolfsberg (89).

Wahl's (86) values were derived from the curve "best" fitting the

TABLE XXIX

Z_p Values for Masses 84 to 89 in Thermal-Neutron Fission of U^{233}

Author	Masses	84	85	86	87	88	89
Wahl (86)[a]				34.41			
Wahl (86)[b]				34.14 ±0.23			
Fiedler (87)[c]		33.50	33.95	34.44	34.88	35.32	35.81
Fiedler (87)[d]		33.64	34.06	34.50	34.87	35.31	35.77
Wolfsberg (89)[b]				34.25 ±0.23			35.86 ±0.08

a. Empirical

b. Measured

c,d. Computed on basis of ECD using final fragment masses and Z_A values from Swiatecki (84) and Seeger (85) respectively

TABLE XXX

Zp Values for Masses 84 to 89 in Thermal-Neutron Fission of U^{235}

Author Masses	84	85	86	87	88	89
Wahl (86)[a]	33.31	33.68	34.10	34.52	34.51	35.37
Wahl (86)[b]			33.91 ±0.25			35.42 ±0.12
Fiedler (87)[c]	33.18	33.61	33.98	34.41	34.88	35.31
Fiedler (87)[d]	33.30	33.70	34.06	34.48	34.90	35.28

a. Empirical

b. Measured

c,d. Computed on basis of ECD using final masses of fragments and Z_A values from Swiatecki (84) and Seeger (85) respectively.

measured data. The curve has no theoretical basis but does provide yields which are consistent with the measured values.

Fiedler's (87) values were calculated using as their basis the postulate of equal charge displacement, ECD. Equal charge displacement postulates that the light and heavy fragments in fission are equally displaced from stability, i.e.

$$Z_{A_H} - Z_{P_H} = Z_{A_L} - Z_{P_L}$$

where the Z_A's and Z_P's are the most stable and most probable charges of the heavy and light mass chains respectively. The most probable charge is given by the following

$$Z_P = Z_A - 1/2\ (Z_{A_H} + Z_{A_L} - Z_F)$$

where Z_F is the charge of the fissioning nucleus. Fiedler (87) has calculated Z_P for U^{233} and U^{235}, from values of Z_A derived from mass formulae of Swiatecki (84) and Seeger (85)

Tables XXXI and XXXII give the predicted yields of short-lived bromine isotopes in thermal-neutron fission of U^{233} and U^{235} respectively. These are obtained by multiplication of the relative chain yields by the cumulative yields of the mass chains. The chain yields for U^{233} and U^{235} were obtained from Bidinosti (90) and Farrar (91) respectively.

Table XXXIII gives the relative proportions of primary and secondary bromine isotopes in the fission of U^{235}. The secondary yields were obtained by summation of the primary yields of the precursors.

(89) K. Wolfsberg, Phys. Rev. 137 B929 (1965).

TABLE XXXI

Predicted Primary Yields[a] of Bromine Isotopes in Thermal-Neutron Fission of U^{233}

Z_p Value[c]	Masses / Chain Yields[b]	84 1.97	85 2.54	86 3.30	87 4.61	88 5.54	89 6.15
		C = 0.95					
ECD - Swiatecki		0.11	0.45	1.4	2.6	2.9	1.8
ECD - Seeger		0.14	0.56	1.5	2.6	2.9	1.8
		C = 1.5					
ECD - Swiatecki		0.20	0.56	1.1	2.1	2.4	1.8
ECD - Seeger		0.25	0.64	1.3	2.1	2.4	1.8

a. Yields are in percent.

b. Chain yields by Bidinosti (90).

c. Computed on basis of ECD using final masses of fragments and Z_A values from Swiatecki (84) and Seeger (85) respectively.

TABLE XXXII

Predicted Primary Yields[a] of Bromine Isotopes in Thermal-Neutron Fission of U^{235}

Z_p Value	Masses / Chain Yields[b]	84 1.01	85 1.31	86 2.04	87 2.50	88 3.58	89 4.73
		C = 0.95					
Empirical - Wahl		0.03	0.13	0.50	1.1	2.1	2.3
ECD-Swiatecki[c]		0.02	0.10	0.41	1.0	2.0	2.5
ECD - Seeger[d]		0.03	0.13	0.40	1.1	2.1	2.5
		C = 1.5					
Empirical - Wahl		0.07	0.20	0.55	1.0	1.6	2.0
ECD - Swiatecki[c]		0.06	0.16	0.50	0.9	1.6	2.0
ECD - Seeger[d]		0.07	0.20	0.48	1.0	1.6	2.0

a. Yields are in percent

b. Chain yield by Farrar (91).

c,d. Computed on basis of ECD using final fragment masses and Z_A values from Swiatecki (84) and Seeger (85) respectively.

TABLE XXXIII

Predicted Proportions of Primary and Secondary Bromine in Thermal-Neutron Fission of U^{235}*

Mass Chain Yield (%)	84 1.01	85 1.31	86 2.04	87 2.50	88 3.58	89 4.73
	C = 0.95					
Primary Yield (%)	0.03	0.13	0.50	1.1	2.0	2.3
Secondary Yield (%)	0.98	1.16	1.51	1.25	0.9	0.4
Secondary / Primary	34.8	9.2	3.0	1.1	0.45	0.15
	C = 1.5					
Primary Yield (%)	0.07	0.20	0.55	1.0	1.6	2.0
Secondary Yield (%)	0.94	1.13	1.41	1.3	1.1	0.6
Secondary / Primary	13.9	6.9	2.6	1.3	0.68	0.33

* Calculation based upon empirical Z_p of Wahl et al (86).

Chain Yield by Farrar (91).

(90) D. R. Bidinosti, D. E. Irish and R. H. Tomlinson, Can. J. Chem. 39 628 (1961).

(91) H. Farrar, H. B. Fickel and R.H.Tomlinson, Can. J. Phys. 40 1017 (1962).